for the gastrula organizer and its derivatives. BMC Genomics *9*, 511.

22. Suzuki, D., Yamada, A., Amano, T., Yasuhara, R., Kimura, A., Sakahara, M., Tsumaki, N., Takeda, S., Tamura, M., Nakamura, M., et al. (2009). Essential mesenchymal role of small GTPase Rac1 in interdigital programmed cell death during limb development. Dev. Biol. *335*, 396–406.
23. Kimura, S., and Shiota, K. (1996). Sequential changes of programmed cell death in developing fetal mouse limbs and its possible roles in limb morphogenesis. J. Morphol. *229*, 337–346.
24. Sernagor, E., Eglen, S.J., and Wong, R.O. (2001). Development of retinal ganglion cell structure and function. Prog. Retin. Eye Res. *20*, 139–174.
25. Bandyopadhyay, A., Tsuji, K., Cox, K., Harfe, B.D., Rosen, V., and Tabin, C.J. (2006). Genetic analysis of the roles of BMP2, BMP4, and BMP7 in limb patterning and skeletogenesis. PLoS Genet. *2*, e216.
26. Robert, B. (2007). Bone morphogenetic protein signaling in limb outgrowth and patterning. Dev. Growth Differ. *49*, 455–468.
27. Dudley, A.T., Lyons, K.M., and Robertson, E.J. (1995). A requirement for bone morphogenetic protein-7 during development of the mammalian kidney and eye. Genes Dev. *9*, 2795–2807.
28. Khokha, M.K., Hsu, D., Brunet, L.J., Dionne, M.S., and Harland, R.M. (2003). Gremlin is the BMP antagonist required for maintenance of Shh and Fgf signals during limb patterning. Nat. Genet. *34*, 303–307.
29. Furuta, Y., and Hogan, B.L. (1998). BMP4 is essential for lens induction in the mouse embryo. Genes Dev. *12*, 3764–3775.
30. Asai-Coakwell, M., French, C.R., Berry, K.M., Ye, M., Koss, R., Somerville, M., Mueller, R., van Heyningen, V., Waskiewicz, A.J., and Lehmann, O.J. (2007). GDF6, a novel locus for a spectrum of ocular developmental anomalies. Am. J. Hum. Genet. *80*, 306–315.
31. Tassabehji, M., Fang, Z.M., Hilton, E.N., McGaughran, J., Zhao, Z., de Bock, C.E., Howard, E., Malass, M., Donnai, D., Diwan, A., et al. (2008). Mutations in GDF6 are associated with vertebral segmentation defects in Klippel-Feil syndrome. Hum. Mutat. *29*, 1017–1027.
32. Wyatt, A.W., Osborne, R.J., Stewart, H., and Ragge, N.K. (2010). Bone morphogenetic protein 7 (BMP7) mutations are associated with variable ocular, brain, ear, palate, and skeletal anomalies. Hum. Mutat. *31*, 781–787.
33. Ye, M., Berry-Wynne, K.M., Asai-Coakwell, M., Sundaresan, P., Footz, T., French, C.R., Abitbol, M., Fleisch, V.C., Corbett, N., Allison, W.T., et al. (2010). Mutation of the bone morphogenetic protein GDF3 causes ocular and skeletal anomalies. Hum. Mol. Genet. *19*, 287–298.
34. Zhou, F., Leder, P., Zuniga, A., and Dettenhofer, M. (2009). Formin1 disruption confers oligodactylism and alters Bmp signaling. Hum. Mol. Genet. *18*, 2472–2482.
35. Chang, B., Smith, R.S., Peters, M., Savinova, O.V., Hawes, N.L., Zabaleta, A., Nusinowitz, S., Martin, J.E., Davisson, M.L., Cepko, C.L., et al. (2001). Haploinsufficient Bmp4 ocular phenotypes include anterior segment dysgenesis with elevated intraocular pressure. BMC Genet. *2*, 18.
36. Ragge, N.K., Brown, A.G., Poloschek, C.M., Lorenz, B., Henderson, R.A., Clarke, M.P., Russell-Eggitt, I., Fielder, A., Gerrelli, D., Martinez-Barbera, J.P., et al. (2005). Heterozygous mutations of OTX2 cause severe ocular malformations. Am. J. Hum. Genet. *76*, 1008–1022.
37. Behesti, H., Papaioannou, V.E., and Sowden, J.C. (2009). Loss of Tbx2 delays optic vesicle invagination leading to small optic cups. Dev. Biol. *333*, 360–372.

REPORT

Mutations in *POLR3A* and *POLR3B* Encoding RNA Polymerase III Subunits Cause an Autosomal-Recessive Hypomyelinating Leukoencephalopathy

Hirotomo Saitsu,[1,*] Hitoshi Osaka,[2] Masayuki Sasaki,[3] Jun-ichi Takanashi,[4] Keisuke Hamada,[5] Akio Yamashita,[6] Hidehiro Shibayama,[7] Masaaki Shiina,[5] Yukiko Kondo,[1] Kiyomi Nishiyama,[1] Yoshinori Tsurusaki,[1] Noriko Miyake,[1] Hiroshi Doi,[1] Kazuhiro Ogata,[5] Ken Inoue,[8] and Naomichi Matsumoto[1,*]

Congenital hypomyelinating disorders are a heterogeneous group of inherited leukoencephalopathies characterized by abnormal myelin formation. We have recently reported a hypomyelinating syndrome characterized by diffuse cerebral hypomyelination with cerebellar atrophy and hypoplasia of the corpus callosum (HCAHC). We performed whole-exome sequencing of three unrelated individuals with HCAHC and identified compound heterozygous mutations in *POLR3B* in two individuals. The mutations include a nonsense mutation, a splice-site mutation, and two missense mutations at evolutionally conserved amino acids. Using reverse transcription-PCR and sequencing, we demonstrated that the splice-site mutation caused deletion of exon 18 from *POLR3B* mRNA and that the transcript harboring the nonsense mutation underwent nonsense-mediated mRNA decay. We also identified compound heterozygous missense mutations in *POLR3A* in the remaining individual. *POLR3A* and *POLR3B* encode the largest and second largest subunits of RNA Polymerase III (Pol III), RPC1 and RPC2, respectively. RPC1 and RPC2 together form the active center of the polymerase and contribute to the catalytic activity of the polymerase. Pol III is involved in the transcription of small noncoding RNAs, such as 5S ribosomal RNA and all transfer RNAs (tRNA). We hypothesize that perturbation of Pol III target transcription, especially of tRNAs, could be a common pathological mechanism underlying *POLR3A* and *POLR3B* mutations.

Congenital hypomyelinating disorders form a heterogeneous group of central nervous system leukoencephalopathies that is characterized by abnormal myelin formation. Although these conditions are readily recognized by brain magnetic resonance imaging (MRI), many cases are not diagnosed correctly.[1] Several syndromes affecting myelination, such as hypomyelination with hypodontia and hypogonadotropic hypogonadism (4H) syndrome (MIM 612440) and hypomyelination with atrophy of the basal ganglia and cerebellum (H-ABC) (MIM 612438), have been described.[2–5] We have recently reported a hypomyelinating syndrome characterized by diffuse cerebral hypomyelination with cerebellar atrophy and hypoplasia of the corpus callosum (HCAHC).[6] Individuals with HCAHC do not show hypodontia or atrophy of the basal ganglia, which are observed in 4H syndrome and H-ABC; however, diffuse hypomyelination, atrophy, or hypoplasia of the cerebellum and corpus callosum are overlapping features of these three syndromes, suggesting that there might be a common underlying pathological mechanism.

Here, we report on four individuals with HCAHC from three unrelated families (Figure 1A; Table 1). Clinical information and peripheral blood or saliva samples were obtained from the family members after obtaining written informed consent. Experimental protocols were approved by the Institutional Review Board of Yokohama City University. To identify pathogenic mutations, we performed whole-exome sequencing of three probands from three unrelated families (individuals 1, 3, and 4). DNAs were captured with the SureSelect Human All Exon 50Mb Kit (Agilent Technologies, Santa Clara, CA) and sequenced with one lane per sample on an Illumina GAIIx (Illumina, San Diego, CA) with 108 bp paired-end reads. Image analysis and base calling were performed by sequence control software real-time analysis and CASAVA software v1.7 (Illumina). A total of 90,014,368 (individual 1), 86,942,264 (individual 3), and 92,168,758 (individual 4) paired-end reads were obtained and aligned to the human reference genome sequence (GRCh37/hg19) with MAQ[7] and NextGENe software v2.00 with sequence condensation by consolidation (SoftGenetics, State College, PA). This approach resulted in more than 88% of target exomes being covered by ten reads or more (see Table S1, available online). Single nucleotide variants (SNVs) were called with MAQ and NextGENe. Small insertions and deletions were

[1]Department of Human Genetics, Yokohama City University Graduate School of Medicine, 3-9 Fukuura, Kanazawa-ku, Yokohama 236-0004, Japan; [2]Division of Neurology, Clinical Research Institute, Kanagawa Children's Medical Center, 2-138-4 Mutsukawa, Minami-ku, Yokohama 232-8555, Japan; [3]Department of Child Neurology, National Center of Neurology and Psychiatry, 4-1-1 Ogawahigashi-cho Kodaira, Tokyo 187-8551, Japan; [4]Department of Pediatrics, Kameda Medical Center, 929 Higashi-cho, Kamogawa-shi, Chiba 296-8602, Japan; [5]Department of Biochemistry, Yokohama City University Graduate School of Medicine, 3-9 Fukuura, Kanazawa-ku, Yokohama 236-0004, Japan; [6]Department of Molecular Biology, Yokohama City University Graduate School of Medicine, 3-9 Fukuura, Kanazawa-ku, Yokohama 236-0004, Japan; [7]Department of Neurology, Kameda Medical Center, 929 Higashi-cho, Kamogawa-shi, Chiba 296-8602, Japan; [8]Department of Mental Retardation and Birth Defect Research, National Institute of Neuroscience, National Center of Neurology and Psychiatry, 4-1-1 Ogawahigashi-cho Kodaira, Tokyo 187-8551, Japan
*Correspondence: hsaitsu@yokohama-cu.ac.jp (H.S.), naomat@yokohama-cu.ac.jp (N.M.)
DOI 10.1016/j.ajhg.2011.10.003.

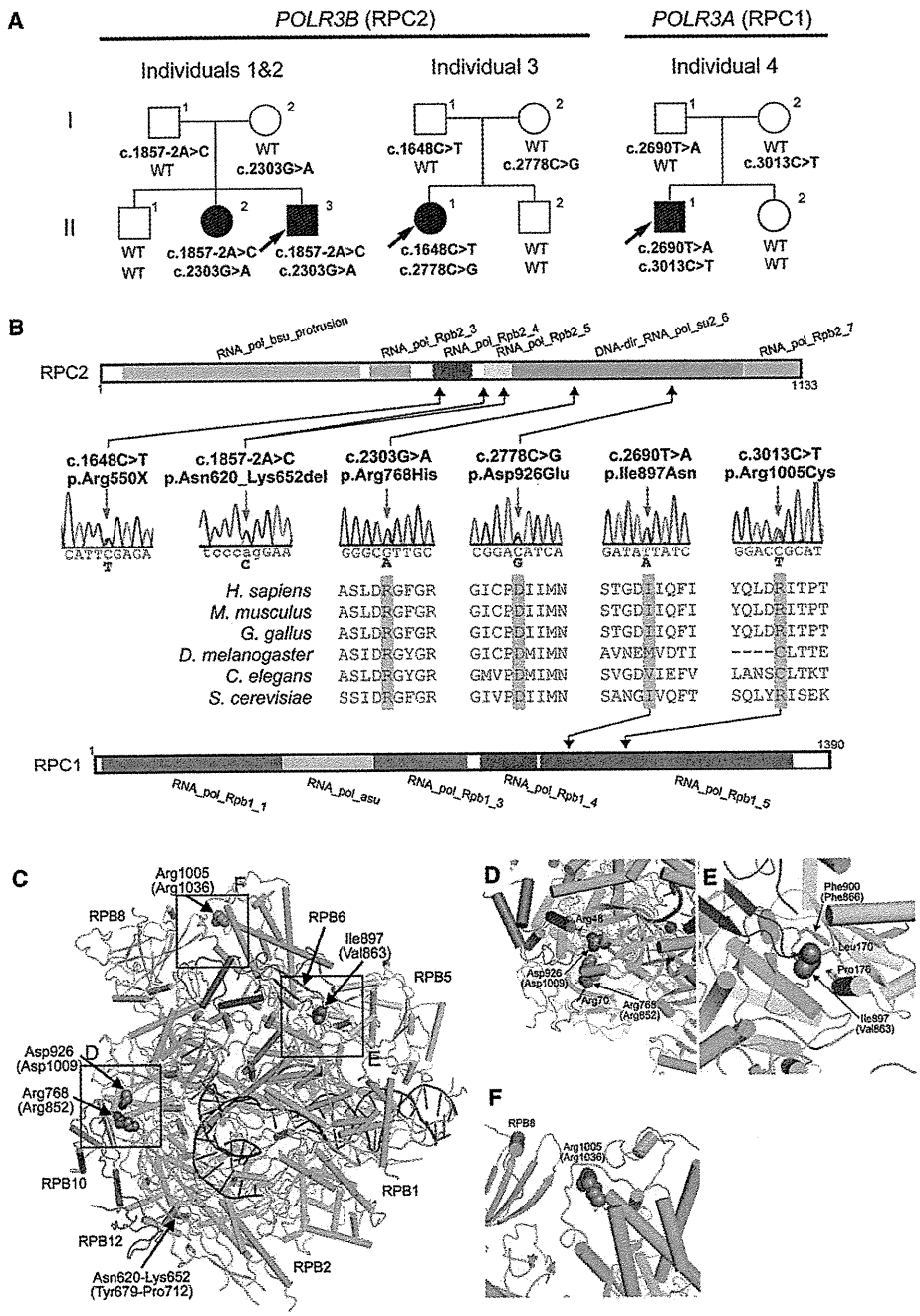

Figure 1. Mutations in *POLR3B* and *POLR3A*

(A) Pedigrees of four kindreds with HCAHC are shown. We identified four mutations in *POLR3B* encoding RPC2 in three individuals from two unrelated families and two mutations in *POLR3A* encoding RPC1 in one family. The segregation of each mutation is shown.

(B) Schematic representation of RPC2 (upper) and RPC1 (lower) proteins with Pfam domains (from Ensembl). Locations of each amino-acid-altering mutation are depicted with electropherograms. All of the missense mutations occurred at evolutionally conserved amino acids. Homologous sequences were aligned with the CLUSTALW website.

(C–F) 3D representations of RPC1 and RPC2 mutations. Mutated amino acids in RPC1 and RPC2 are shown along with their equivalent positions in the homologous RPB1 and RPB2 subunits of RNA Polymerase II (amino acid and its position in parenthesis). The structure and positions of mutations are illustrated by PyMOL with the crystal structure (PDB accession number 3GTP). RPB3, RPB9, and RPB11 subunits, which are specific to RNA Polymerase II, have been omitted from the figure. RPB1 is shown in green, RPB2 in sky blue, RPB5 in yellow, RPB6 in dark blue, RPB8 in pink, RPB10 in orange, RPB12 in purple, DNA in brown, and RNA in red. Amino acids that interact with mutated amino acids are also shown.

Table 1. Clinical Features of the Individuals

Clinical Features	Individual 1	Individual 2	Individual 3	Individual 4
Genes	*POLR3B*	*POLR3B*	*POLR3B*	*POLR3A*
Mutations, DNA	c.1857-2A>C, c.2303G>A	c.1857-2A>C, c.2303G>A	c.1648C>T, c.2778C>G	c.2690T>A, c.3013C>T
Mutations, protein	p.Asn620_Lys652del, p.Arg768His	p.Asn620_Lys652del, p.Arg768His	p.Arg550X, p.Asp926Glu	p.Ile897Asn, p.Arg1005Cys
Gender	M	F	F	M
Current age (years)	27	30	16	17
Intellectual disability	mild	mild	moderate	mild
Cognitive regression	–	–	–	–
Seizures	–	–	–	–
Initial motor development	normal	normal	normal	normal
Age of onset (years)	3	3	2	4
Motor deterioration	–	–	–	+
Wheelchair use	–	–	–	+
Optic atrophy	–	–	–	–
Myopia	+	+	–	+
Nystagmus	+	+	–	–
Abnormal pursuit	+	+	+	–
Vertical gaze limitation	+	+	+	–
Dysphagia	–	–	+	–
Hypersalivation	–	–	–	–
Cerebellar signs	+	+	+	+
Tremor	–	+	+	+
Babinski refex	–	–	–	–
Spasticity	–	–	mild	–
Peripheral nerve involvement	–	–	–	–
Nerve biopsy	NA	NA	NA	NA
Hypodontia	–	–	–	–
Hypogonadism	+	+	–	–

NA is an abbreviation for not available.

detected with NextGENe. Called SNVs were annotated with SeattleSeq Annotation.

We adopted a prioritization scheme to identify the pathogenic mutation in each individual, similar to the approach taken by recent studies (Table S2).[8–10] First, we excluded the variants registered in the dbSNP131 or 1000 Genome Project from all the detected variants. Then, SNVs commonly detected by MAQ and NextGENe analyses were selected as highly confident variants; 364 to 374 SNVs of nonsynonymous (NS) or canonical splice-site (SP) changes, along with 113 to 124 small insertions or deletions (indels), were identified per individual. We also excluded variants found in our 55 in-house exomes, which are derived from 12 healthy individuals and 43 individuals with unrelated diseases, reducing the number of candidate variants to ~250 per individual. Assuming that HCAHC is an autosomal-recessive disorder based on two affected individuals in one pedigree (individuals 1 and 2), we focused on rare heterozygous variants that are not registered in the dbSNP or in our in-house 55 exomes.

We surveyed all genes in each individual for two or more NS, SP, or indel variants. We found three to eight candidate genes per individual (Table S2). Among them, only *POLR3B* encoding RPC2, the second largest subunit of RNA Polymerase III (Pol III), was common in two individuals (individuals 1 and 3). The inheritance of the variants in *POLR3B* (transcript variant 1, NM_018082.5) was examined by Sanger sequencing. In individual 1, we confirmed that a canonical splice-site mutation (c.1857-2A>C [p.Asn620_Lys652del]), 2 bp upstream of exon 18, was

inherited from his father, and that a missense mutation (c.2303G>A [p.Arg768His]) in exon 21 were inherited from his mother (Figure 1A). The two mutations were also present in an affected elder sister (individual 2) but not present in a healthy elder brother. In individual 3, we confirmed that a nonsense mutation (c.1648C>T [p.Arg550X]) in exon 16 was inherited from her father and that a missense mutation (c.2778C>G [p.Asp926Glu]) in exon 24 was inherited from her mother (Figure 1A). The two mutations were not present in a healthy younger brother. To examine the mutational effects of c.1857-2A>C and c.1648C>T, reverse transcription PCR and sequencing with total RNA extracted from lymphoblastoid cells derived from the individuals was performed as previously described.[11] We demonstrated that the c.1857-2A>C mutation caused deletion of exon 18 from the *POLR3B* mRNA (Figures 2A–2C), resulting in an in-frame 33 amino acid deletion (p.Asn620_Lys652del) from RPC2 (Figure 1B). In addition, the mutated transcript harboring the nonsense mutation (c.1648C>T) was found to be expressed at a much lower level compared with the wild-type transcript (Figure 2D). The expression level of the mutated transcript was increased after treatment with 30 μM cycloheximide (CHX),[11] which inhibits nonsense-mediated mRNA decay (NMD), indicating that the mutant transcript underwent NMD (Figure 2D). The two missense mutations (p.Arg768His and p.Asp926Glu) found in the three individuals occurred at evolutionary conserved amino acids (Figure 1B). Among the other candidate genes in individuals 1 and 3, *MSLN* (MIM 601051), encoding mesothelin isoform 1 preproprotein that is cleaved into megakaryocyte potentiating factor and mesothelin, is a potential candidate in the family of individual 1 as its homozygous variant segregated with the phenotype; however, it is expressed in epithelial mesotheliomas, and the mutation affects less conserved amino acid (Table S3). The other candidate genes' variants did not cosegregate with the phenotype. Thus, mutations in *POLR3B* are most likely to cause HCAHC in two families.

In individual 4, in whom no *POLR3B* mutations were found, there were six candidate genes for an autosomal-recessive model. Among them, *POLR3A* (MIM 614258, GenBank accession number NM_007055.3), harboring two missense mutations, appeared to be a primary candidate because it encodes the largest subunit of Pol III (RPC1) (Figure 1A and Table S2). By Sanger sequencing, we confirmed that a missense mutation (c.2690T>A [p.Ile897Asn]) in exon 20 was inherited from his father and that another missense mutation (c.3013C>T [p.Arg1005Cys]) in exon 23 was inherited from his mother (Figure 1A). The two mutations were not present in a healthy younger sister. The two missense mutations (p.Ile897Asn and p.Arg1005Cys) occurred at relatively conserved amino acids (Figure 1B). In total, we found four mutations in *POLR3B* and two mutations in *POLR3A*. Evaluation of the missense mutations by PolyPhen-2 program showed that three mutations (p.Arg768His,

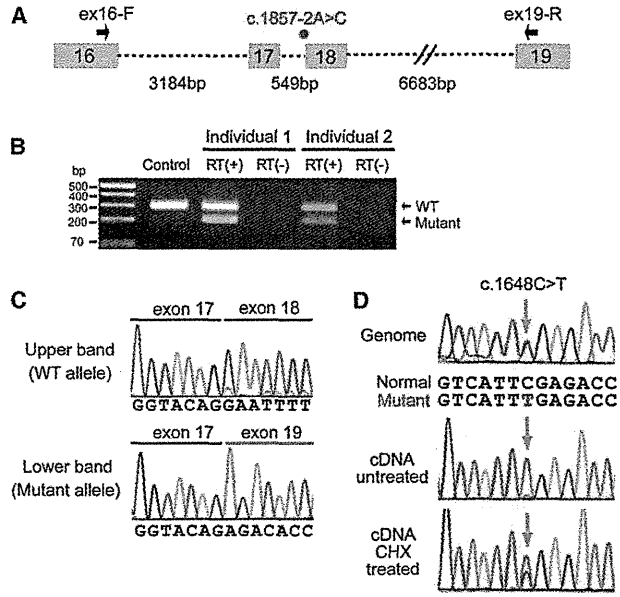

Figure 2. Effects of Splice-Site and Nonsense Mutations in *POLR3B*

(A) Schematic representation of the genomic structure of *POLR3B* from exon 16 to 19. Exons, introns, and primers are shown by boxes, dashed lines, and arrows, respectively. The mutation in intron 17 is depicted as a red dot.

(B) RT-PCR analysis of individuals 1 and 2 with c.1857-2A>C and a normal control. Two PCR products were detected from the individual's cDNA: the upper band is the wild-type (WT) transcript, and the lower band is the mutant. Only a single wild-type amplicon was detected in the control.

(C) Sequence of WT and mutant amplicons clearly showed exon 18 skipping in the mutant allele.

(D) Analysis of the c.1648C>T mutation. Sequence of PCR products amplified with genomic (upper), cDNA from untreated cells (middle), and cDNA from CHX treated cells (lower) as a template. Although untreated cells show extremely low levels of c.1648C>T mutant allele expression, cells treated to inhibit NMD show significantly increased levels of mutant allele expression.

p.Asp926Glu, and p.Ile897Asn) were probably damaging and that p.Arg1005Cys is tolerable. The c.2303G>A mutation (*POLR3B*) was found in one allele out of 540 Japanese control chromosomes. The remaining five mutations were not detected in 540 Japanese control chromosomes, indicating that the mutations are very rare in the Japanese population. Among the other candidate genes in individuals 4, *IGSF10*, a member of immunoglobulin superfamily, is a potential candidate because its variants segregated with the phenotype (Table S3); however, considering a close relationship between *POLR3A* and *POLR3B*, and the fact that *POLR3A* mutations have been recently reported in hypomyelinating leukodystrophy (see below),[12] *POLR3A* abnormality is the most plausible culprit for HCAHC in individual 4.

The structure of Pol III[13,14] and Pol II[15,16] is highly homologous, especially in the largest subunits. Thus, we extrapolated the mutations of RPC1 or RPC2 onto the structure of yeast Pol II (Protein Data Bank [PDB] accession number 3GTP)[17] (Figure 1C). RPB1 and RPB2 subunits of

yeast Pol II are homologous to RPC1 and RPC2 of Pol III, respectively. Asn620_Lys652 in RPC2 corresponds to Tyr679_Lys712 in RPB2. The deletion of Asn620_Lys652 (Tyr679_Lys712) would destroy a structural core of RPB2, leading to loss of RPB2 function. In addition, Arg768 (Arg852 in RPB2) interacts with the main-chain carbonyl group of Arg70 of the RPB12 subunit, and Asp926 (Asp1009 in RPB2) interacts with the side chain of Arg48 of the RPB10 subunit of Pol II (Figure 1D). Arg768His (Arg852His) and Asp926Glu (Asp1009Glu) substitutions are considered to disturb these subunit interactions, leading to dysfunction of the polymerase. Therefore, structural prediction suggests that the mutations in *POLR3B* (RPC2) could affect Pol III function. On the other hand, Ile897 and Arg1005 in RPC1 correspond to Val863 and Arg1036 in RPB1, respectively. Ile897 (Val863) has hydrophobic interactions with Leu170 and Pro176 of the RPB5 subunit and with Phe900 (Phe866) of the RPB1 subunit of Pol II (Figure 1E). Ile897Asn (Val863Asn) substitution is likely to disturb this interaction. Arg1005 (Arg1036) stabilizes interaction between RPB1 and RPB8 subunits (Figure 1F). The Arg1005Cys (Arg1036Cys) substitution appears to make this interaction unstable. Thus mutations in *POLR3A* are also predicted to affect Pol III function.

Clinical features of individuals with *POLR3A* or *POLR3B* mutations are presented in Table 1. MRI revealed high-intensity areas in the white matter in T2-weighted images, cerebellar atrophy, and a hypoplastic corpus callosum in all four individuals (Figure 3). Individuals 1 and 2 showed an extremely similar clinical course. They developed normally during their early infancy, i.e., walking unaided at 15 and 14 months, and uttering a few words at 12 and 13 months, respectively. After the age of 3, individual 1 presented with unstable walking and frequent stumbling and falling down, and individual 2 became poor at exercise. They both had severe myopia (corrected visual acuity of 0.7 and 0.5 at most, respectively). They graduated from elementary, junior high, and high schools with poor records, and the intelligence quotient (IQ) of individual 2 was 52 (WAIS-III). In individual 1, unstable walking was prominent at around 18 years, and he could not ride a bicycle because of ataxia; however, he could drive an automobile. Amenorrhea was noted in individual 2, and was successfully treated by hormone therapy. Individual 1 showed several signs of hypogonadism, including absence of underarm and mustache hair, thin pubic hair (Tanner II), and serum levels of testosterone, follicle stimulating hormone, and luteinizing hormone that were below normal for age 27. Neurological examination of both individuals revealed mild horizontal nystagmus, slowing of smooth-pursuit eye movement, and gaze limitation, especially in vertical gazing, hypotonia, mildly exaggerated deep-tendon reflex (patellar and Achilles tendon reflex) with negative Babinski reflex, and cerebellar signs and symptoms, including ataxic speech, wide-based ataxic gait, dysdiadochokinesis, and dysmetria. Clinical information for individual 3 has been reported previously.[6] Additional findings are as follows: slowing of smooth-pursuit eye movement, gaze limitation in vertical gazing, normal auditory brain responses (ABR), cerebral symptoms with mild spasticity, and intellectual disability (an IQ of 43 according to the WISC-III test), and no myopia but hypermetropic astigmatism. She showed no deterioration besides a mild dysphagia and walks herself to a school for the disabled. Individual 4 developed normally during his

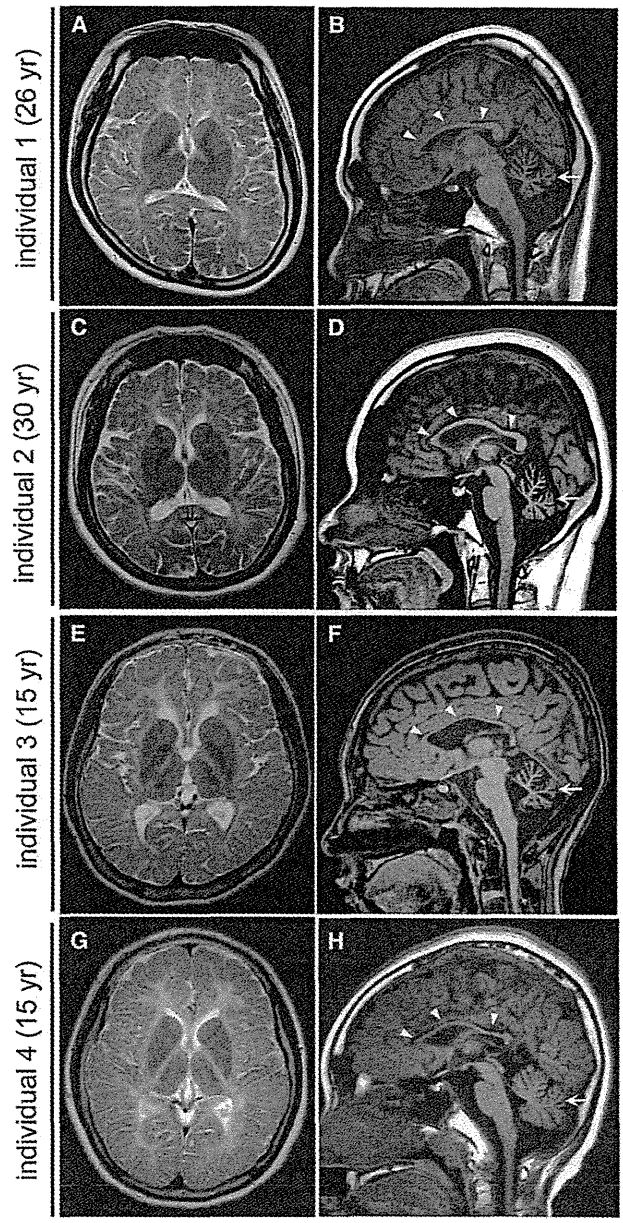

Figure 3. Brain MRI of Individuals with *POLR3B* and *POLR3A* Mutations

(A, C, E, and G) T2-weighted axial images through the basal ganglia. High-intensity areas in the white matter were observed in all individuals.

(B, D, F, and H) T1-weighted midline sagittal images. All the individuals showed hypoplastic corpus callosum (arrowheads) and atrophy of cerebellum (arrows).

early infancy, had normal head control at 3 months, was speaking a few words at 12 months, and was walking unaided at 14 months. His parents noted mild tremors around 4 years. He had normal stature, weight, and head circumference. Although he had severe myopia, his eye movement was smooth with no limitation or nystagmus. He had sensory neuronal deafness on the left side. He showed normal muscle tone and had no spasticity or rigidity. His tendon reflexes were slightly elevated with a negative Babinski reflex. Cerebellar signs were noted; expressive ataxic explosive speech, intension tremor, poor finger to nose test, dysdiadochokinesis, dysmetria, and wide-based ataxic gait. His intelligence quotient was 57 (according to the WISC-III test). His peripheral nerve conduction velocity was within the normal range and his ABR showed normal responses on the right side. He suffered motor deterioration around age 14 and became wheelchair bound.

In this study, we successfully identified compound heterozygous mutations in *POLR3A* and *POLR3B* in individuals with HCAHC. Very recently, Bernard et al.[12] reported that *POLR3A* mutations cause three overlapping leukodystrophies, including 4H syndrome, suggesting that HCAHC is, at least in part, within a wide clinical spectrum caused by *POLR3A* mutations. The p.Arg1005Cys mutation was shared between individual 9 in their report and our individual 4. All 19 individuals with *POLR3A* mutations showed progressive upper motor neuron dysfunction and cognitive regression. In addition, individual 9 showed abnormal eye movement, hypodontia, and hypogonadism. None of these features were recognized in our individual 4; these differences further support phenotypic variability of *POLR3A* mutations.[12] Given the phenotypic similarities among 4H syndrome, HCAHC, and H-ABC, there is a possibility that H-ABC is also allelic and caused by recessive mutations in either *POLR3A* or *POLR3B*.

Pol III consists of 17 subunits and is involved in the transcription of small noncoding RNAs, such as 5S ribosomal RNA (rRNA), U6 small nuclear RNA (snRNA), 7SL RNA, RNase P, RNase MRP, short interspersed nuclear elements (SINEs), and all transfer RNAs (tRNAs). Pol III-transcribed genes are classified into three types based on promoter elements and transcription factors. 5S rRNA is a solo type I gene. Type II genes include tRNA, 7SL RNA, and SINEs. Type III genes include U6 snRNA, RNase P, and RNase MRP.[18–20] The Pol III system is important for cell growth in yeast, and its transcription is tightly regulated during the cell cycle.[20] In zebrafish, *polr3b* mutant larvae that have a deletion of 41 conserved amino acids (Δ239-279) from the Rpc2 protein showed a proliferation deficit in multiple tissues, including intestine, endocrine pancreas, liver, retina and terminal branchial arches.[21] In the mutants, the expression levels of tRNA were significantly reduced, whereas the level of 5S rRNA expression was not changed, suggesting that this *polr3b* mutation can differentially affect Pol III target promoters.[21] RPC2 contributes to the catalytic activity of the polymerase and forms the active center of the polymerase together with the largest subunit, RPC1.[22] Thus, it is reasonable to consider that mutations in *POLR3A* and *POLR3B* cause overlapping phenotypes. Indeed, three individuals with *POLR3B* mutations showed diffuse cerebral hypomyelination, atrophy of the cerebellum and corpus callosum, and abnormal eye movements that overlap with *POLR3A* abnormalities.[12] Furthermore, two out of three individuals showed hypogonadism, suggesting a common pathological mechanism between *POLR3A* and *POLR3B* mutations. In the zebrafish *polr3b* mutants there were no defects of the central nervous system other than a reduced size of the retina, probably reflecting species differences; however, the reduced level of tRNA in the *polr3b* mutants raises the possibility that defects of tRNA transcription by Pol III could be a common pathological mechanism underlying *POLR3A* and *POLR3B* mutations. Supporting this idea, mutations in two genes involved in aminoacylation activity of tRNA synthetase cause defects of myelination in central nervous system: *DARS2* (MIM 610956) and *AIMP* (MIM 603605).[23,24] In addition, mutations in four genes encoding aminoacyl-tRNA synthetase cause Charcot-Marie-Tooth disease (MIM 613641, 613287, 601472, and 608323), resulting from demyelination of peripheral nerve axons: *KARS* (MIM 601421), *GARS* (MIM 600287), *YARS* (MIM 603623), and *AARS* (MIM 601065).[25–28] Thus, it is very likely that regulation of tRNA expression is essential for development and maintenance of myelination in both central and peripheral nervous systems.

An interesting clinical feature of *POLR3B* mutations is the absence of motor deterioration. All three individuals with *POLR3B* mutations could walk without support at ages 16, 27, and 30, whereas individual 3 with *POLR3A* mutations had motor deterioration around age 14. Bernard et al.[12] also reported progressive upper motor neuron dysfunction and cognitive regression in individuals with *POLR3A* mutations. Thus, there is a possibility that phenotypes caused by *POLR3A* mutations could be more severe and progressive than *POLR3B* mutant phenotypes. Identification of a greater number of cases with *POLR3B* mutations is required to confirm this hypothesis.

In conclusion, our data, together with that of a previous report,[12] demonstrate that mutations in Pol III subunits cause overlapping autosomal-recessive hypomyelinating disorders. Establishment of an animal model will facilitate our understanding of the pathophysiology of the multiple defects caused by Pol III mutations.

Supplemental Data

Supplemental Data include three tables and can be found with this article online at http://www.cell.com/AJHG/.

Acknowledgments

We would like to thank all the individuals and their families for their participation in this study. This work was supported by

research grants from the Ministry of Health, Labour, and Welfare (H.S., H.O., M.S., J.T., N. Miyake, K.I. and N. Matsumoto), the Japan Science and Technology Agency (N. Matsumoto), a Grant-in-Aid for Scientific Research on Innovative Areas (Foundation of Synapse and Neurocircuit Pathology) from the Ministry of Education, Culture, Sports, Science and Technology of Japan (N. Matsumoto), a Grant-in-Aid for Scientific Research from Japan Society for the Promotion of Science (H.O., N. Matsumoto), a Grant-in-Aid for Young Scientist from Japan Society for the Promotion of Science (H.S.). This work has been done at Advanced Medical Research Center, Yokohama City University.

Received: August 31, 2011
Revised: October 5, 2011
Accepted: October 10, 2011
Published online: October 27, 2011

Web Resources

The URLs for data presented herein are as follows:

ClustalW, http://www.genome.jp/tools/clustalw/
dbSNP, http://www.ncbi.nlm.nih.gov/projects/SNP/
Ensembl, http://uswest.ensembl.org/index.html
GenBank, http://www.ncbi.nlm.nih.gov/Genbank/
Online Mendelian Inheritance in Man, http://www.omim.org
PolyPhen-2, http://genetics.bwh.harvard.edu/pph2/
Protein Data Bank, http://www.pdb.org/pdb/home/home.do
PyMOL, http://www.pymol.org/
SeattleSeq Annotation, http://gvs.gs.washington.edu/SeattleSeq Annotation/

References

1. Schiffmann, R., and van der Knaap, M.S. (2009). Invited article: an MRI-based approach to the diagnosis of white matter disorders. Neurology *72*, 750–759.
2. Timmons, M., Tsokos, M., Asab, M.A., Seminara, S.B., Zirzow, G.C., Kaneski, C.R., Heiss, J.D., van der Knaap, M.S., Vanier, M.T., Schiffmann, R., and Wong, K. (2006). Peripheral and central hypomyelination with hypogonadotropic hypogonadism and hypodontia. Neurology *67*, 2066–2069.
3. Wolf, N.I., Harting, I., Boltshauser, E., Wiegand, G., Koch, M.J., Schmitt-Mechelke, T., Martin, E., Zschocke, J., Uhlenberg, B., Hoffmann, G.F., et al. (2005). Leukoencephalopathy with ataxia, hypodontia, and hypomyelination. Neurology *64*, 1461–1464.
4. Wolf, N.I., Harting, I., Innes, A.M., Patzer, S., Zeitler, P., Schneider, A., Wolff, A., Baier, K., Zschocke, J., Ebinger, F., et al. (2007). Ataxia, delayed dentition and hypomyelination: a novel leukoencephalopathy. Neuropediatrics *38*, 64–70.
5. van der Knaap, M.S., Naidu, S., Pouwels, P.J., Bonavita, S., van Coster, R., Lagae, L., Sperner, J., Surtees, R., Schiffmann, R., and Valk, J. (2002). New syndrome characterized by hypomyelination with atrophy of the basal ganglia and cerebellum. AJNR Am. J. Neuroradiol. *23*, 1466–1474.
6. Sasaki, M., Takanashi, J., Tada, H., Sakuma, H., Furushima, W., and Sato, N. (2009). Diffuse cerebral hypomyelination with cerebellar atrophy and hypoplasia of the corpus callosum. Brain Dev. *31*, 582–587.
7. Li, H., Ruan, J., and Durbin, R. (2008). Mapping short DNA sequencing reads and calling variants using mapping quality scores. Genome Res. *18*, 1851–1858.
8. Doi, H., Yoshida, K., Yasuda, T., Fukuda, M., Fukuda, Y., Morita, H., Ikeda, S., Kato, R., Tsurusaki, Y., Miyake, N., et al. (2011). Exome sequencing reveals a homozygous *SYT14* mutation in adult-onset, autosomal-recessive spinocerebellar ataxia with psychomotor retardation. Am. J. Hum. Genet. *89*, 320–327.
9. Pierce, S.B., Walsh, T., Chisholm, K.M., Lee, M.K., Thornton, A.M., Fiumara, A., Opitz, J.M., Levy-Lahad, E., Klevit, R.E., and King, M.C. (2010). Mutations in the DBP-deficiency protein HSD17B4 cause ovarian dysgenesis, hearing loss, and ataxia of Perrault Syndrome. Am. J. Hum. Genet. *87*, 282–288.
10. Gilissen, C., Arts, H.H., Hoischen, A., Spruijt, L., Mans, D.A., Arts, P., van Lier, B., Steehouwer, M., van Reeuwijk, J., Kant, S.G., et al. (2010). Exome sequencing identifies *WDR35* variants involved in Sensenbrenner syndrome. Am. J. Hum. Genet. *87*, 418–423.
11. Saitsu, H., Kato, M., Okada, I., Orii, K.E., Higuchi, T., Hoshino, H., Kubota, M., Arai, H., Tagawa, T., Kimura, S., et al. (2010). *STXBP1* mutations in early infantile epileptic encephalopathy with suppression-burst pattern. Epilepsia *51*, 2397–2405.
12. Bernard, G., Chouery, E., Putorti, M.L., Tetreault, M., Takanohashi, A., Carosso, G., Clement, I., Boespflug-Tanguy, O., Rodriguez, D., Delague, V., et al. (2011). Mutations of *POLR3A* Encoding a Catalytic Subunit of RNA Polymerase Pol III Cause a Recessive Hypomyelinating Leukodystrophy. Am. J. Hum. Genet. *89*, 415–423.
13. Jasiak, A.J., Armache, K.J., Martens, B., Jansen, R.P., and Cramer, P. (2006). Structural biology of RNA polymerase III: subcomplex C17/25 X-ray structure and 11 subunit enzyme model. Mol. Cell *23*, 71–81.
14. Fernández-Tornero, C., Böttcher, B., Riva, M., Carles, C., Steuerwald, U., Ruigrok, R.W., Sentenac, A., Müller, C.W., and Schoehn, G. (2007). Insights into transcription initiation and termination from the electron microscopy structure of yeast RNA polymerase III. Mol. Cell *25*, 813–823.
15. Cramer, P., Bushnell, D.A., and Kornberg, R.D. (2001). Structural basis of transcription: RNA polymerase II at 2.8 angstrom resolution. Science *292*, 1863–1876.
16. Gnatt, A.L., Cramer, P., Fu, J., Bushnell, D.A., and Kornberg, R.D. (2001). Structural basis of transcription: an RNA polymerase II elongation complex at 3.3 A resolution. Science *292*, 1876–1882.
17. Wang, D., Bushnell, D.A., Huang, X., Westover, K.D., Levitt, M., and Kornberg, R.D. (2009). Structural basis of transcription: backtracked RNA polymerase II at 3.4 angstrom resolution. Science *324*, 1203–1206.
18. Oler, A.J., Alla, R.K., Roberts, D.N., Wong, A., Hollenhorst, P.C., Chandler, K.J., Cassiday, P.A., Nelson, C.A., Hagedorn, C.H., Graves, B.J., and Cairns, B.R. (2010). Human RNA polymerase III transcriptomes and relationships to Pol II promoter chromatin and enhancer-binding factors. Nat. Struct. Mol. Biol. *17*, 620–628.
19. Dieci, G., Fiorino, G., Castelnuovo, M., Teichmann, M., and Pagano, A. (2007). The expanding RNA polymerase III transcriptome. Trends Genet. *23*, 614–622.
20. Dumay-Odelot, H., Durrieu-Gaillard, S., Da Silva, D., Roeder, R.G., and Teichmann, M. (2010). Cell growth- and differentiation-dependent regulation of RNA polymerase III transcription. Cell Cycle *9*, 3687–3699.

21. Yee, N.S., Gong, W., Huang, Y., Lorent, K., Dolan, A.C., Maraia, R.J., and Pack, M. (2007). Mutation of RNA Pol III subunit *rpc2/polr3b* Leads to Deficiency of Subunit Rpc11 and disrupts zebrafish digestive development. PLoS Biol. *5*, e312.
22. Werner, M., Thuriaux, P., and Soutourina, J. (2009). Structure-function analysis of RNA polymerases I and III. Curr. Opin. Struct. Biol. *19*, 740–745.
23. Scheper, G.C., van der Klok, T., van Andel, R.J., van Berkel, C.G., Sissler, M., Smet, J., Muravina, T.I., Serkov, S.V., Uziel, G., Bugiani, M., et al. (2007). Mitochondrial aspartyl-tRNA synthetase deficiency causes leukoencephalopathy with brain stem and spinal cord involvement and lactate elevation. Nat. Genet. *39*, 534–539.
24. Feinstein, M., Markus, B., Noyman, I., Shalev, H., Flusser, H., Shelef, I., Liani-Leibson, K., Shorer, Z., Cohen, I., Khateeb, S., et al. (2010). Pelizaeus-Merzbacher-like disease caused by AIMP1/p43 homozygous mutation. Am. J. Hum. Genet. *87*, 820–828.
25. Latour, P., Thauvin-Robinet, C., Baudelet-Méry, C., Soichot, P., Cusin, V., Faivre, L., Locatelli, M.C., Mayençon, M., Sarcey, A., Broussolle, E., et al. (2010). A major determinant for binding and aminoacylation of tRNA(Ala) in cytoplasmic Alanyl-tRNA synthetase is mutated in dominant axonal Charcot-Marie-Tooth disease. Am. J. Hum. Genet. *86*, 77–82.
26. McLaughlin, H.M., Sakaguchi, R., Liu, C., Igarashi, T., Pehlivan, D., Chu, K., Iyer, R., Cruz, P., Cherukuri, P.F., Hansen, N.F., et al. (2010). Compound heterozygosity for loss-of-function lysyl-tRNA synthetase mutations in a patient with peripheral neuropathy. Am. J. Hum. Genet. *87*, 560–566.
27. Antonellis, A., Ellsworth, R.E., Sambuughin, N., Puls, I., Abel, A., Lee-Lin, S.Q., Jordanova, A., Kremensky, I., Christodoulou, K., Middleton, L.T., et al. (2003). Glycyl tRNA synthetase mutations in Charcot-Marie-Tooth disease type 2D and distal spinal muscular atrophy type V. Am. J. Hum. Genet. *72*, 1293–1299.
28. Jordanova, A., Irobi, J., Thomas, F.P., Van Dijck, P., Meerschaert, K., Dewil, M., Dierick, I., Jacobs, A., De Vriendt, E., Guergueltcheva, V., et al. (2006). Disrupted function and axonal distribution of mutant tyrosyl-tRNA synthetase in dominant intermediate Charcot-Marie-Tooth neuropathy. Nat. Genet. *38*, 197–202.

REPORT

Exome Sequencing Reveals a Homozygous *SYT14* Mutation in Adult-Onset, Autosomal-Recessive Spinocerebellar Ataxia with Psychomotor Retardation

Hiroshi Doi,[1,2] Kunihiro Yoshida,[3] Takao Yasuda,[4] Mitsunori Fukuda,[4] Yoko Fukuda,[5] Hiroshi Morita,[6] Shu-ichi Ikeda,[6] Rumiko Kato,[7] Yoshinori Tsurusaki,[1] Noriko Miyake,[1] Hirotomo Saitsu,[1] Haruya Sakai,[1] Satoko Miyatake,[1] Masaaki Shiina,[8] Nobuyuki Nukina,[9] Shigeru Koyano,[2] Shoji Tsuji,[5] Yoshiyuki Kuroiwa,[2] and Naomichi Matsumoto[1,*]

Autosomal-recessive cerebellar ataxias (ARCAs) are clinically and genetically heterogeneous disorders associated with diverse neurological and nonneurological features that occur before the age of 20. Currently, mutations in more than 20 genes have been identified, but approximately half of the ARCA patients remain genetically unresolved. In this report, we describe a Japanese family in which two siblings have slow progression of a type of ARCA with psychomotor retardation. Using whole-exome sequencing combined with homozygosity mapping, we identified a homozygous missense mutation in *SYT14*, encoding synaptotagmin XIV (SYT14). Expression analysis of the mRNA of *SYT14* by a TaqMan assay confirmed that *SYT14* mRNA was highly expressed in human fetal and adult brain tissue as well as in the mouse brain (especially in the cerebellum). In an in vitro overexpression system, the mutant SYT14 showed intracellular localization different from that of the wild-type. An immunohistochemical analysis clearly showed that SYT14 is specifically localized to Purkinje cells of the cerebellum in humans and mice. Synaptotagmins are associated with exocytosis of secretory vesicles (including synaptic vesicles), indicating that the alteration of the membrane-trafficking machinery by the *SYT14* mutation may represent a distinct pathomechanism associated with human neurodegenerative disorders.

Hereditary ataxias are genetically heterogeneous neurological disorders: autosomal-dominant, autosomal-recessive, X-linked, and mitochondrial types are known. Among ataxias, spinocerebellar ataxia (SCA) is relatively common and involves the cerebellum, brainstem, or spinocerebellar long tracts.[1] Autosomal-recessive cerebellar ataxias (ARCAs) are generally associated with diverse neurological and nonneurological attributes, resulting in complex phenotypes. ARCAs include congenital nonprogressive ataxias and progressive ataxias such as SCAs.[2] The clinical onset of ARCAs usually occurs before the age of 20, even if congenital types are excluded.[1,3,4] Currently, more than 20 defective genes have been identified in ARCAs.[2,5,6] These genes have variable recognized functions, including those involving mitochondrial energy generation, cellular metabolisms, DNA repair, chaperone-mediated protein folding, RNA processing, and ion channels.[1,3,6] Approximately half of the patients with ARCAs remain genetically unresolved.[4] Therefore, more investigations of ARCAs are required. In this study, we describe a Japanese family with two siblings showing psychomotor retardation and the slowly progressive type of SCA without involvement of pyramidal tracts or peripheral nerves. Exome sequencing combined with homozygosity mapping successfully identified a causative mutation.

Clinical information and blood materials were obtained from the family members after written informed consent was secured. Experimental protocols were approved by IRBs of the Yokohama City University and the Shinshu University. Among the children of first-cousin parents, two siblings (IV-3 and IV-4) were found to be affected, whereas the other two (IV-1 and IV-2) were healthy (Figure 1A). No similar patients were recognized within the family. IV-3 had mild psychomotor retardation from childhood. He found a job after graduating from an ordinary junior high school. At 35 years of age, he lost his job for social reasons. Although he had some gait disturbances from childhood, he could independently go shopping and walk a dog even after leaving his occupation. At the age of ~56, he developed obvious gait unsteadiness and began to stumble frequently. At 58, he started to choke on food. These symptoms gradually worsened, and he sought medical examination at 59 years of age. He displayed disturbances of smooth-pursuit eye movements, dysarthria, mild limb ataxia, and moderate truncal ataxia. His muscle tone was normal, and no involuntary

[1]Department of Human Genetics, Graduate School of Medicine, Yokohama City University, 3-9 Fukuura, Kanazawa-ku, Yokohama 236-0004, Japan; [2]Department of Clinical Neurology and Stroke Medicine, Graduate School of Medicine, Yokohama City University, 3-9 Fukuura, Kanazawa-ku, Yokohama 236-0004, Japan; [3]Division of Neurogenetics, Department of Brain Disease Reseach, Shinshu University School of Medicine, 3-1-1 Asahi, Matsumoto, Nagano 390-8621, Japan; [4]Laboratory of Membrane Trafficking Mechanisms, Department of Developmental Biology and Neuroscience, Graduate School of Life Sciences, Tohoku University, Aobayama, Aoba-ku, Sendai, Miyagi 980-8578, Japan; [5]Department of Neurology, Graduate School of Medicine, The University of Tokyo, 7-3-1 Hongo, Bunkyo-ku, Tokyo 113-8655, Japan; [6]Department of Medicine (Neurology & Rheumatology), Shinshu University School of Medicine, 3-1-1 Asahi, Matsumoto, Nagano 390-8621, Japan; [7]Department of Pediatrics, National Higashi-Saitama Hospital, 4147 Kurohama, Hasuda 349-0196, Japan; [8]Department of Biochemistry, Graduate School of Medicine, Yokohama City University, 3-9 Fukuura, Kanazawa-ku, Yokohama 236-0004, Japan; [9]Laboratory for Structural Neuropathology, Brain Science Institute, RIKEN, 2-1 Hirosawa, Wako 351-0198, Japan
*Correspondence: naomat@yokohama-cu.ac.jp
DOI 10.1016/j.ajhg.2011.07.012.

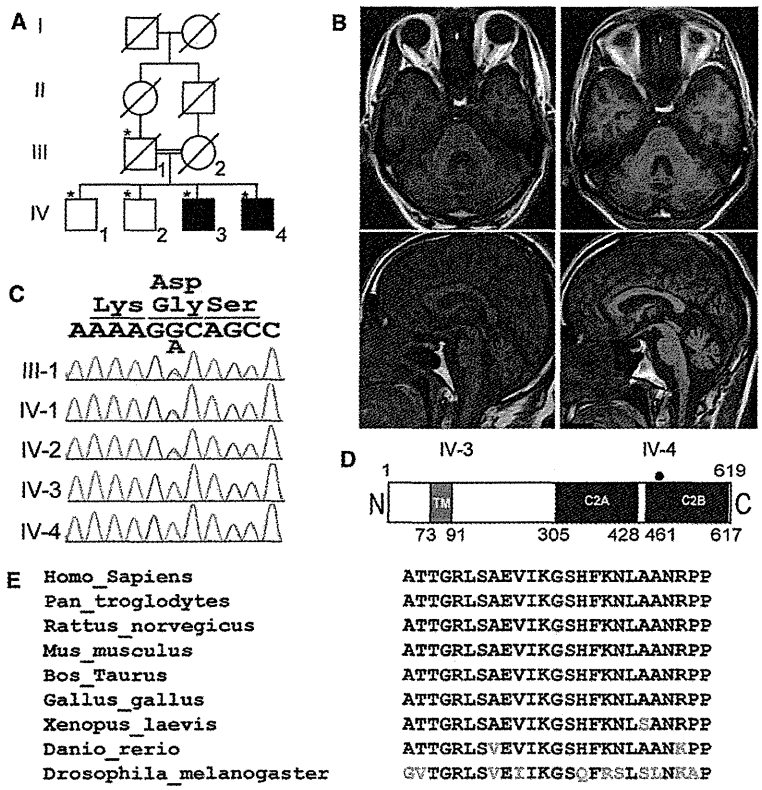

Figure 1. Familial Pedigree, Brain MRI of Patients, and the *SYT14* Mutation Identified
(A) Familial pedigree of the patients with autosomal-recessive spinocerebellar ataxia. *An asterisk indicates members whose genomic DNA was available for this study.
(B) Brain MRI of IV-3 at 59 years of age (left panels) and IV-4 at 56 years of age (right panels). Axial (upper panels) and sagittal (lower panels) sections of a T1-weighted image are shown.
(C) Electropherograms of unaffected (III-1, IV-1, and IV-2) and affected (IV-3 and IV-4) members, who show the mutation.
(D) Schematic presentation of SYT14. The red dot indicates the location of the mutation in the C2B domain.
(E) The missense mutation occurred at an evolutionarily conserved amino acid (in red).

movements were observed. Laboratory examination, including analysis of serum albumin, vitamin E, and α-fetoprotein, was normal. A nerve-conduction study (NCS) indicated no neuropathy. No retinitis pigmentosa was recognized by ophthalmologic evaluation. Brain magnetic resonance imaging (MRI) revealed mild atrophy of the cerebellar vermis and hemispheres but no apparent atrophy of the brain stem or the cerebral cortex. (Figure 1B, left panels).

Similar to IV-3, IV-4 also had psychomotor retardation from childhood, but this retardation was more severe than that of IV-3. After graduation from a school for disabled children at the age of 15, he entered a facility for disabled people. He showed gait disorder, but he was able to walk without a cane. At an age of ~50, his gait disturbance worsened, and he went for a medical check at a hospital when he was 56 years old. He displayed disturbance of smooth-pursuit eye movements, gaze-evoked horizontal nystagmus, dysarthria, mild limb ataxia, and moderate truncal ataxia. No involuntary movements were observed. His laboratory tests, including those for serum albumin, vitamin E, and α-fetoprotein, were normal. NCS was normal. A brain MRI was similar to that of IV-3 (Figure 1B, right panels). The clinical manifestations of these two patients are summarized in Table 1.

To search for the disease locus, we conducted genome-wide SNP genotyping of III-1, IV-1, IV-2, IV-3, and IV-4 by using the Genome-wide Human SNP Array 6.0 (SNP 6.0 array) (Affymetrix, Inc., Santa Clara, CA) according to the manufacturer's instructions. Then, SNP 6.0 array data were subjected to homozygosity mapping with HomozygosityMapper software.[7] For the linkage analysis, a subset of 7339 SNPs with high heterozygosity (mean heterozygosity 0.49) was extracted from the SNP 6.0 array data with the program Linkdatagen, for which the bin size was set to 0.5cM and the allele frequency of the Japanese population was used.[8] The multipoint LOD score was calculated with Allegro version 2[9] on the basis of the model of autosomal-recessive and X-linked-recessive inheritance, respectively. In both models, complete penetrance and a disease-allele frequency of 0.0001 were adopted. The homozygosity mapping revealed a total of three regions, which together were approximately 11.35 Mb in size, as candidate loci, where genes known to be mutated in ARCA did not exist (Table 2). In the model of autosomal-recessive inheritance, a total of ten regions with a LOD score greater than 1.5 in the multipoint linkage analysis were identified (Table S1). The three homozygous regions in accordance with the linked regions still survived as candidate regions. On the basis of X-linked recessive inheritance, a total of three regions with positive LOD scores (maximum LOD score = 0.9031) were highlighted; together, these three regions were approximately 101.03 Mb (Table S1).

To find a gene mutation within the candidate loci, we performed whole-exome sequencing on IV-3 and IV-4. Three micrograms of genomic DNA was processed with the SureSelect Human All Exon Kit v.1 (approximately 180,000 exons covering 38 Mb of the CCDS database) (Agilent Technologies, Santa Clara, CA) according to the manufacturer's instructions. Captured DNAs were sequenced on an Illumina GAIIx (Illumina, San Diego, CA) with 76 bp pair-end reads. Of the possible eight lanes of the flow cell, two lanes for IV-3 and three lanes for IV-4 (Illumina) were used. Image analysis and base calling

Table 1. Clinical Features of the Patients

Clinical Features	IV-3	IV-4
Age at present	61	58
Sex	male	male
Age of obvious ataxia	56	around 50
Mental retardation	mild	moderate
Ocular apraxia	no	no
Ophthalmoplegia	no	no
Nystagmus	no	+
Dysarthria	+	+
Truncal ataxia	++	++
Limb ataxia	+	+
Extrapyramidal signs	no	no
Involuntary movements	no	no
Sensory involvements	no	no
Tendon reflex	normal-increased	normal-decreased
Plantar responses	normal	normal
Peripheral neuropathy	no	no
Pes cavus	no	no
SARA[a]	12/40	15/40
Cerebellar atrophy on MRI	+	+
others	normal level of serum albumin, vitamin E, and α-fetoprotein	normal level of serum albumin, vitamin E, and α-fetoprotein

[a] SARA: Scale for the assessment and rating of ataxia.[32]

Table 2. Regions of Homozygosity

Chromosome	Chromosomal Position (rsID)	Size (Mb)	LOD
1	207226930 (rs2761781)–213992561 (rs1857229)	6.77	2.0537
4	181929079 (rs918401)–185188999 (rs7690914)	3.26	2.0554
22	45676443 (rs3905396)–47003473 (rs2013591)	1.33	2.0545

Regions of homozygosity were identified by HomozygosityMapper, and the LOD scores were calculated by multipoint linkage analysis, for which SNPs were extracted from SNP 6.0 array data via Linkdatagen.

were performed by sequence control software (SCS) real-time analysis (Illumina) and CASAVA software v1.6 (Illumina). Reads were aligned to the human reference genome sequence (UCSC hg18, NCBI build 36.1) via the ELAND v2 program (Illumina). Coverage was calculated statistically with a script created by BITS (Tokyo, Japan). Approximately 71 million reads from IV-3 and 148 million reads from IV-4 (these numbers of reads passed quality-control [Path Filter]) were mapped to the human reference genome with Mapping and Assembly with Qualities (MAQ)[10] and NextGENe software v2.00 (SoftGenetics, State College, PA) under the default settings. MAQ aligned 59,491,138 and 126,159,746 reads to the whole genome for IV-3 and IV-4, respectively. A script created by BITS was used for extraction of SNPs and indels from the alignment data; dbSNP build 130 served as a reference for registered SNPs. A consensus quality score of 40 or more was adopted for the SNP analysis in MAQ. Coverage analysis revealed that 65.0% (IV-3) and 71.3% (IV-4) of the coding sequences (CDS) were completely covered (100%), and 77.7% (IV-3) and 80.3% (IV-4) of CDS were mostly covered by reads (90% or more) through the whole genome. 79.0% (IV-3) and 79.7% (IV-4) of total CDS were covered by ten reads or more (50 reads or more in 66.4% and 77.1%, respectively).

To identify the pathogenic mutation, we adopted a prioritization scheme, which has been used in recent studies.[11–13] First, we excluded the variants registered in dbSNP130 from all the detected variants and then picked up homozygous mutations and variants in coding regions and the intronic regions within 50 bp from coding sequences. Of the homozygous mutations and variants, we focused on those within the candidate regions. As a result, only two missense mutations or variants, p.Gly484Asp (c.1451G>A) (NM_001146261.1) in exon 8 of *SYT14* (1q32.2, [MIM 610949]) and p.Gln4203Arg (c.12608A>G) (NM_206933.2) in exon 63 of *USH2A* (1q41, [MIM 608400]) remained as candidates for both cases (Table S2). Sanger sequencing with ABI 3500xL (Life Technologies, Carlsbad, CA) confirmed that the c.1451G>A of *SYT14* was homozygous in IV-3 and IV-4 and heterozygous in III-1 (father), IV-1, and IV-2, whereas the c.12608A>G of *USH2A* was homozygous in IV-2 as well as IV-3 and IV-4 (Figure 1C and data not shown). The *SYT14* missense mutation occurred at an evolutionarily conserved amino acid among different species and resides in the second C2 (C2B) domain (Figures 1D and 1E). In silico analysis incorporating different tools, including Polyphen, Polyphen2, SIFT, and Align GVGD, consistently indicated that the change was damaging (Table S3). The mutation was not detected in 576 Japanese control chromosomes, indicating that the mutation is very rare. On the basis of the X-linked recessive model, no pathological hemizygous mutation of protein-coding genes was detected in the possible candidate loci (Table S4).

We considered the *SYT14* mutation to be the causative agent and used the Sanger method to conduct mutation screening of all the coding regions of *SYT14* in 65 simplex SCA cases and 37 SCA familial cases, including three with autosomal-recessive inheritance. Only p.Gly183Glu (c.548G>A) was found in one family with autosomal-dominant SCA; however, the change was not consistent with the SCA phenotype in the family (Table S3). Thus, we could not detect any other pathological changes in *SYT14*. This was probably due to the small number of cases tested.

Synaptotagmin XIV (SYT14), which is encoded by *SYT14*, is a member of the synaptotagmins (SYTs), which are membrane-trafficking proteins, and SYT14 is conserved across many organisms.[14] Although the original report indicated that *SYT14* was not expressed in mouse brain,[14] multiple lines of evidence, including from the Allen brain Atlas, suggest that *SYT14* is expressed in the central nervous system (CNS) of the fly, mouse, and human brains.[15,16] To confirm *SYT14* expression in the CNS, we performed TaqMan quantitative real-time PCR analysis with cDNAs of adult human tissue (Human MTC Panel I, #636742) (Clontech Laboratories, Mountain View, CA), fetal human tissue (Human Fetal MTC Panel, #636747) (Clontech Laboratories), mouse tissue (Mouse MTC Panel I, #636745) (Clontech Laboratories), and various regions of the mouse brain (GSMBRSET) (NIPPON Genetics, Tokyo, Japan) as templates. Predesigned TaqMan probe sets for human *SYT14* (Hs00950169_m1), mouse *Syt14* (Mm00805319_m1), human *β-actin* (*ACTB*, 4326315E), and mouse *Actb* (43522341E) from Applied Biosystems were used. PCR reactions (total volume of 20 μl) contained 10 μl of the TaqMan Gene Expression Master Mix (Applied Biosystems), 1 μl of 20 × TaqMan reagents for *ACTB/Actb* and *SYT14/Syt14*, and 1 μl of cDNA (containing 1 ng cDNA in MTC panels and 25 ng cDNA in GSMBRSET) as the template. PCR was performed on a Rotor-Gene Q (QIAGEN, Valencia, CA) as follows: 2 min at 50°C and 10 min at 95°C, then 40 cycles of 95°C for 15 s and 60°C for 1 min. Expression levels were calculated with the Rotor-Gene Q Series Software (QIAGEN) by the $2^{-\Delta\Delta Ct}$ method. The cycling threshold (Ct) of the target gene was compared with the Ct of *ACTB* cDNA, and ΔCt was expressed as Ct of *SYT14* − Ct of *ACTB*. ΔΔCt was expressed as ΔCt of the control sample − ΔCt of each sample, and relative concentration was determined as $2^{-\Delta\Delta Ct}$. Expression in the kidney and the cerebral cortex was used as the control in Figures 2A–2D. *SYT14* was predominantly expressed in human adult and fetal brain tissues (Figures 2A and 2B). Even in mice, substantial expression in the brain was confirmed (but, not predominant) (Figure 2C). Among various brain regions in mice, *SYT14* was mostly expressed in the cerebellum (Figure 2D).

Intracellular distribution of SYT14 in cultured cells was investigated. The full-length *SYT14* PCR product amplified from human brain cDNA (MHS4426-99239810, Open Biosystems, Huntsville, AL) was used as a template and subcloned into pDONR221 (the entry vector of Gateway system, Invitrogen). We used site-directed mutagenesis to produce the *SYT14* mutant and variants by using a mutagenesis kit (Toyobo, Osaka, Japan). Variants include c.611C>T and c.810_812del, which are registered in dbSNP130, and c.548G>A, which was detected in an SCA patient with autosomal-dominant inheritance but did not segregate with the phenotype, indicating that it is nonpathogenic (Table S3). All constructs were verified by DNA sequencing. Each construct was recloned into the pEF-DEST51 mammalian expression vector (Invitrogen) and transfected to COS-1 cells with the FuGENE^{R}6 transfection reagent (Roche Applied Science, Mannheim, Germany) according to the manufacturer's instructions. Localization of the mutant (p.Gly484Asp) was clearly different from that of the wild-type and other (normal) variants. Whereas the wild-type and other variants were localized to the perinuclear and submembranous regions, p.Gly484Asp was localized in the cytoplasm (significant amounts were in the perinuclear region) but formed a characteristic reticular pattern without showing any submembranous distribution (Figures 2E and S2B). Confocal microscopic analysis showed that the p.Gly484Asp mutant was colocalized with an endoplasmic reticulum (ER) marker, protein disulfide isomerase (PDI), throughout the cells, whereas the wild-type colocalized with PDI dominantly in perinuclear regions (Figure 2F). immunoblot analysis combined with subcellular fractionation of the transfected cells further confirmed that the mutant was distributed differently from the wild-type. The wild-type and the mutant (p.Gly484Asp) were distributed in the nucleus and Golgi apparatus fractions; however, only the mutant was detected in microsome fractions containing ER fragments together with an ER membrane marker, calnexin (Figure S1).[17] These data suggest that improper folding of the mutant protein results in abnormal retention in the ER.

To investigate the effect of the p.Gly484Asp mutation in the C2B domain on phospholipid binding activity, we amplified cDNA of C2B domains from the wild-type and the p.Gly484Asp mutant from SYT14-expressing vectors by using the following primers: sense, 5′-GGATCCGAAA GTACATCCTCATGTCA-3′; and antisense, 5′-TCATGAC TCTAGCAACGCAT-3′. We then recloned the cDNA into *Escherichia coli* (*E. coli*) expressing vector (pGEX-4T-3). The C2B domain of SYT14 fused to glutathione S-transferase (GST) was expressed in *E. coli* JM109 and purified by standard protocols. Both GST-SYT14-C2B (WT) and GST-SYT14-C2B (p.Gly484Asp) could be mostly purified of contamination by degradation products, but the amount of GST-SYT14-C2B (p.Gly484Asp) obtained was at least four times smaller than that of GST-SYT14-C2B (WT) (data not shown). Liposome (phosphatidylcholine and phosphatidylserine, 1:1, w/w) cosedimentation assay with purified GST-SYT14-C2B was performed as described previously.[18] The result showed that the SYT14-C2B (p.Gly484Asp) bound liposomes similarly to SYT14-C2B (WT) (Figure 2G), indicating that the p.Gly484Asp mutation had no effect on the Ca^{2+}-independent phospholipid-binding activity of the SYT14-C2B domain.

The Allen Mouse Brain Atlas indicates that *Syt14* is expressed in Purkinje cells of the cerebellum in mice; however, SYT14 localization has not been fully investigated.[15] A rabbit polyclonal anti-SYT14 antibody (Ab-SYT14) was generated for immunoblotting and immunocytochemistry (Operon Biotechnologies, Tokyo, Japan) (Figure S2). Immunohistochemical analysis of mouse and human brains was

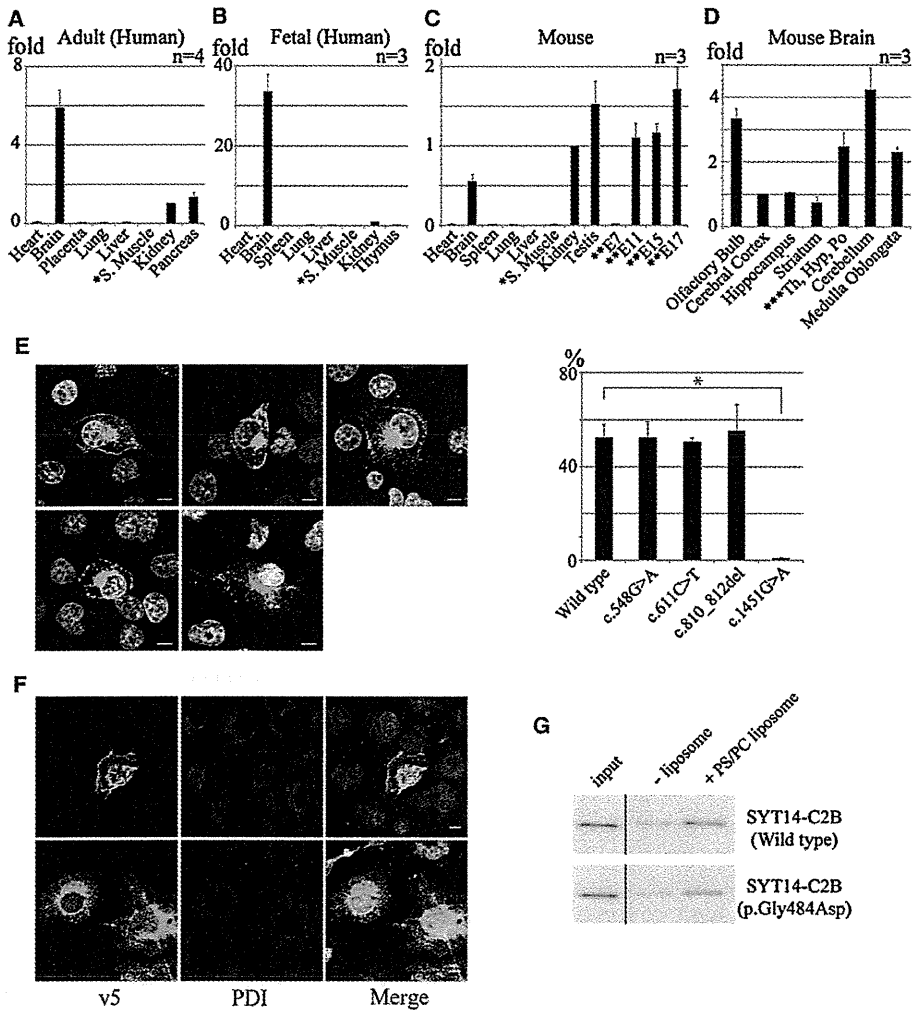

Figure 2. Expression Studies of *SYT14/Syt14* cDNA in Human and Mouse Tissues and Localization of SYT14 in Transfected COS-1 Cells
(A–D) The results of a TaqMan quantitative real-time PCR assay in which the first-strand cDNA of human adult tissues (A), human fetal tissues (B), mouse tissues (C), and various regions of mouse brain (D) were used as templates. The relative cDNA concentrations were determined from cDNA concentrations of the kidney (human adult tissues, human fetal tissues, and mouse tissues) or cerebral cortex (various regions of the mouse brain). Error bars represent the standard deviation. *S. Muscle indicates skeletal muscle. **E7, **E11, **E15, and **E17 indicate mouse embryos at 7, 11, 15, and 17 days of embryonic development, respectively. ***Th, Hyp and Po indicate thalamus, hypothalamus, and pons.
(E) Immunocytochemistry of COS-1 cells transfected with expression vectors of v5/His-tagged wild-type (upper left), p.Gly183Glu (c.548G>A) (upper middle), p.Pro203Leu (c.611C>T) (upper right), p.Glu270del (c.810_812del) (lower left), or p.Gly484Asp (c.1451G>A) (lower middle) SYT14. The SYT14 was detected with the anti-v5 antibody (Alexa fluor 488 as the secondary antibody). Nuclei were stained (white) with 4′,6-diamidino-2-phenylindole (DAPI). The horizontal bars indicate 10 μm. The bar graph indicates the ratio of the cells in which overexpressed proteins were accumulated in submembranous regions. A total of 120 cells per each transfectant in triplicated experiments were counted. Submembranous localization of the mutant (p.Gly484Asp) was mostly unseen, in contrast to the wild-type (*$p < 0.001$).
(F) Immunocytochemical analysis of COS-1 cells transfected with expression vectors of v5/His-tagged wild-type (upper panels) or the p.Gly484Asp mutant (lower panels). The SYT14 was detected with the anti-v5 antibody (Alexa fluor 488 as the secondary antibody), and PDI (protein disulfide isomerase) was visualized with an anti-PDI antibody (Alexa fluor 546 as the secondary antibody). Nuclei were stained (white) with DAPI. The scale bar represents 10 μm. The anti-v5 and anti-PDI antibodies and the Alexa-488-conjugated secondary antibody were all used at a dilution of 1:1000.
(G) Phospholipid binding activity of the C2B domain of the wild-type SYT14 and the p.Gly484Asp mutant. Liposomes and GST-fusion proteins (2 μg) were incubated in 50 mM HEPES-KOH (pH 7.2) in the presence of 2 mM EGTA for 15 min at room temperature. After centrifugation at 12,000 × *g* for 10 min, the supernatants (non-binding fraction) and pellets (phospholipid-binding fraction) were separated as described previously.[18] The pelleted samples and input samples (100 ng) were subjected to 10% SDS-PAGE followed by immunoblotting with horseradish peroxidase-conjugated anti-GST antibody (Santa Cruz Biotechnology, Santa Cruz, CA).

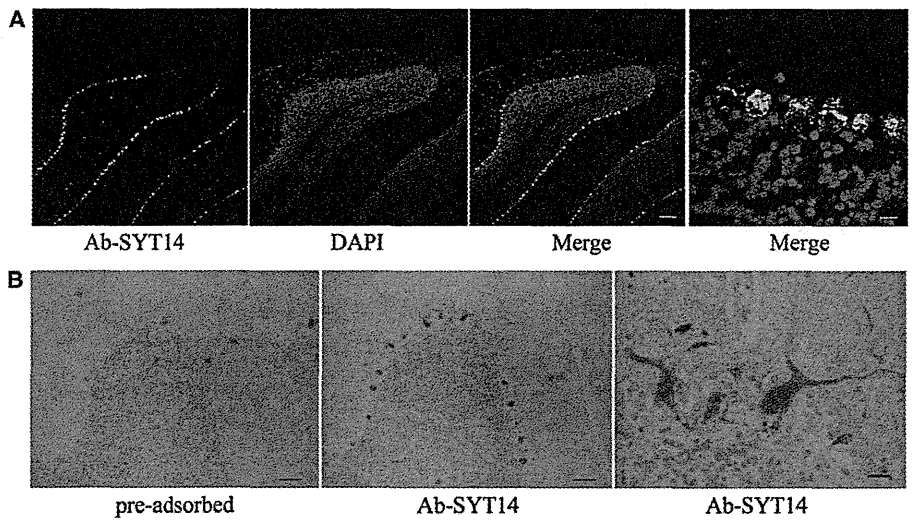

Figure 3. Selective Localization of SYT14 in Purkinje Cells of the Cerebellum in Mice and Humans
(A) Immunohistochemical analysis with the Ab-SYT14 antibody of the cerebellum from an adult mouse at 12 weeks of age. Nuclei were stained with DAPI (the scale bar represents 100 μm). A magnified image is shown in the first right panel (the scale bar represents 10 μm).The Ab-SYT14 antibody (0.9 mg/dl) was used at a dilution ration of 1:2000, and the Alexa-488-conjugated secondary antibody dilution was 1:1000.
(B) Immunohistochemical analysis with the Ab-SYT14 antibody of the cerebellum from the human control. Ab-SYT14 antibodies were preincubated with (left panel) or without (middle panel) peptide antigen before immunostaining. Nuclei were stained with hematoxylin (scale bars represent 100 μm). A magnified image is shown in the right panel (the scale bar represents 20 μm). The Ab-SYT14 antibody (0.9 mg/dl) was used at a dilution of 1:500.

performed with Ab-SYT14, as previously described.[19–21] Mouse brain sections were prepared at the RIKEN Brain Science Institute. Mouse experimental protocols were approved by the animal experiment committee of the RIKEN Brain Science Institute. The frozen brain of C57BL/6J mouse was mounted in Tissue-Tek and sliced to 10 μm sections with a freezing microtome. A human adult brain specimen was obtained through the postmortem examination of a brain from a control subject without neurodegenerative disorders. Informed consent was obtained from the family on the basis of the IRB-approved protocol of Yokohama City University School of Medicine. The human brain was fixed in 10% formalin and cut into 1-cm-thick slices. Sliced tissues were embedded in paraffin wax, and 5 μm sections were immunostained with primary antibodies and visualized with the Vectastain ABC kit (Vector Laboratories, Burlingame, CA). Selective localization of SYT14/Syt14 in Purkinje cells of the mouse cerebellum (Figure 3A) and human cerebellum (Figure 3B) were recognized, indicating that SYT14 plays an important role in the cerebellum. These data are in agreement with a scenario in which the *SYT14* mutation causes cerebellar degeneration in this family.

In this study, only one p.Gly484Asp mutation of *SYT14* was identified in association with SCA. Quintero-Rivera et al.[16] previously described a 12-year-old female with cerebral atrophy, absence seizures, developmental delay with a WISC III score of 58 for full IQ, and de novo t(1;3)(q32.1;q25.1) disrupting *SYT14*. Her brain MRI showed diffuse cerebral atrophy, including that of the cerebellar hemisphere and vermis. Although the inheritance modes are different (recessive impact on our family and dominant on the female patient), mild to moderate mental retardation and cerebellar atrophy are common among patients with *SYT14* abnormalities. It will be important to assess the future phenotype of the female patient studied by Quintero-Rivera et al.[16]

Relatively common ARCAs in Japan include ataxia, early-onset; oculomotor apraxia, hypoalbuminemia/ataxia-oculomotor apraxia 1 (EAOH/AOA1 [MIM 208920]); ataxia-oculomotor apraxia 2 (AOA2 [MIM 606002]); spastic ataxia; Charlevoix-Saguenay type (SACS [MIM 270550]); ataxia with isolated vitamin E deficiency (AVED [MIM 277460]); and ataxia-telangiectasia (AT [MIM 208900]). (Friedrich ataxia 1 [FRDA (MIM 229300)] has never been described in the Japanese population.) In this family, patients never showed ocularmotor apraxia, spasticity, peripheral neuropathy, retinal abnormality, immunological abnormality, or other systemic involvements. As an adult-onset type of pure ARCA, SYNE1-related ARCA (also known as spinocerebellar ataxia, autosomal-recessive 8; SCAR8 [MIM 610743]) is found to be caused by mutations of the gene encoding synaptic nuclear envelope protein 1.[22] Furthermore, these patients were not associated with psychomotor retardation. Thus, SYT14-mutated ARCA, described here, should be categorized to a distinct type of ARCA.

SYTs is a large family of transmembrane proteins associated with exocytosis of secretory vesicles (including synaptic vesicles).[23] The mammalian SYT family is composed

of 17 members. SYTs are anchored to the secretory vesicles via a single transmembrane domain (TM) close to its N terminus and have tandem cytoplasmic domains, C2A and C2B.[24] Among SYTs, SYT1 (MIM 185605) is involved in neurotransmitter release and has been intensively studied. The crystal structure of the C2 domains consists of a compact eight-stranded β-barrel with two protruding loops (loops 1 and 3) that form the Ca^{2+}-binding pockets.[25] SYT1 binds three and two Ca^{2+} ions via loops 1 and 3 of C2A and C2B, respectively. Ca^{2+} binding triggers the rapid penetration of the C2 domains into membranes harboring negatively charged phospholipids. Ca^{2+} also promotes SYT1 binding to t-SNAREs (target-membrane-soluble N-ethylmaleimide-sensitive factor attachment protein receptors). SYT1 is a key sensor for evoked and synchronous neurotransmitter release in many classes of neurons.[23] SYT14 also has TM, C2A, and C2B domains, but it has no conserved Ca^{2+}-binding motif that includes the conserved aspartic acid residues in loops 1 and 3 of C2A and C2B.[26] Although the roles of SYTs as Ca^{2+} sensors have been studied extensively, little is known about Ca^{2+}-independent SYTs, which might inhibit the SNARE-catalyzed fusion in both the absence and presence of Ca^{2+}.[27] Recently, Zhang et al.[28] suggested that Ca^{2+}-independent SYT4 (MIM 600103) negatively regulates exocytosis, regardless of its inability to induce Ca^{2+}-dependent exocytosis.

SYT14 has phospholipid-binding activity that is Ca^{2+} independent.[14] The glycine residue mutated in the family is located around the C2B domain loop 1, which plays an important role in binding to phospholipids in SYT1.[25] We confirmed that, compared to the wild-type, the mutation did not alter the binding activity of SYT14 to phospholipids. In an overexpression system, wild-type SYT14 as well as normal variants were distributed in the cytoplasm close to the plasma membrane, showing in-line accumulation along with the membrane. In contrast, the p.Gly484Asp mutant showed a different (reticular) distribution pattern. In the ER, several cotranslational and posttranslational modifications that are required for the correct folding of transmembrane and secretory proteins take place.[29,30] Incompletely folded proteins are generally excluded from ER exit sites.[29] The fact that the p.Gly484Asp was not properly transferred from the ER suggests that the mutant protein might not fold correctly. The lower yield of the mutant protein as compared to the wild-type in the bacterial expression system we performed also supports the improper folding of the mutant. Abnormal distribution in the ER might result in the loss of function of SYT14 or in ER dysfunction.

In conclusion we have shown that SYT14 is localized specifically in Purkinje cells of mouse and human cerebellum. The results strongly support the involvement of SYT14 in the pathogenesis of SCA and are consistent with the atrophy of the cerebellum seen in both patients. A possible relationship between SYTs and neurodegeneration has been suggested previously,[31] and here we provide data that support the idea that disruption of an SYT protein is involved in human neurodegeneration and that exocytosis machinery can be involved in one of the pathomechanisms of neurodegeneration.

Supplemental Data

Supplemental Data include two figures and five tables and can be found with this article online at http://www.cell.com/AJHG/.

Acknowledgments

We would like to thank the patients and their family for their participation in this study. We are indebted to Syu-ichi Hirai (Department of Molecular Biology, Yokohama City University) for providing useful technical information about subcellular fractionation and to Keiko Yamaoka (Kanagawa Rehabilitation Center) for providing brain tissue from the control subject. This work was supported by research grants from the Ministry of Health, Labour, and Welfare (H.S., N. Miyake, and N. Matsumoto), the Japan Science and Technology Agency (N. Matsumoto), a Grant-in-Aid for Scientific Research from the Japan Society for the Promotion of Science (N. Matsumoto), a Grant-in-Aid for Young Scientist from the Japan Society for the Promotion of Science (H.D., N. Miyake, and H.S.) and a grant-in-aid from The Kimi Imai Memorial Foundation for Research of Incurable Neuromuscular Diseases (H.D.).

Received: June 4, 2011
Revised: July 11, 2011
Accepted: July 15, 2011
Published online: August 11, 2011

Web Resources

The URLs for data presented herein are as follows:

Align GVGD, http://agvgd.iarc.fr/
Allen Human brain Atlas, http://human.brain-map.org/
Allen Mouse Brain Atlas, http://mouse.brain-map.org/
HomozygosityMapper, http://www.homozygositymapper.org/
Online Mendelian Inheritance in Man (OMIM), http://www.omim.org/
PolyPhen, http://genetics.bwh.harvard.edu/pph/
PolyPhen2, http://genetics.bwh.harvard.edu/pph2/
SIFT, http://blocks.fhcrc.org/sift/SIFT.html

Rerefences

1. Fogel, B.L., and Perlman, S. (2007). Clinical features and molecular genetics of autosomal recessive cerebellar ataxias. Lancet Neurol. *6*, 245–257.
2. Palau, F., and Espinós, C. (2006). Autosomal recessive cerebellar ataxias. Orphanet J. Rare Dis. *1*, 47.
3. Embiruçu, E.K., Martyn, M.L., Schlesinger, D., and Kok, F. (2009). Autosomal recessive ataxias: 20 types, and counting. Arq. Neuropsiquiatr. *67*, 1143–1156.
4. Anheim, M., Fleury, M., Monga, B., Laugel, V., Chaigne, D., Rodier, G., Ginglinger, E., Boulay, C., Courtois, S., Drouot, N., et al. (2010). Epidemiological, clinical, paraclinical and

molecular study of a cohort of 102 patients affected with autosomal recessive progressive cerebellar ataxia from Alsace, Eastern France: Implications for clinical management. Neurogenetics *11*, 1–12.
5. Manto, M., and Marmolino, D. (2009). Cerebellar ataxias. Curr. Opin. Neurol. *22*, 419–429.
6. Vermeer, S., Hoischen, A., Meijer, R.P., Gilissen, C., Neveling, K., Wieskamp, N., de Brouwer, A., Koenig, M., Anheim, M., Assoum, M., et al. (2010). Targeted next-generation sequencing of a 12.5 Mb homozygous region reveals *ANO10* mutations in patients with autosomal-recessive cerebellar ataxia. Am. J. Hum. Genet. *87*, 813–819.
7. Seelow, D., Schuelke, M., Hildebrandt, F., and Nurnberg, P. (2009). HomozygosityMapper—An interactive approach to homozygosity mapping. Nucleic Acids Res. *37*, W593–W599.
8. Bahlo, M., and Bromhead, C.J. (2009). Generating linkage mapping files from Affymetrix SNP chip data. Bioinformatics *25*, 1961–1962.
9. Gudbjartsson, D.F., Thorvaldsson, T., Kong, A., Gunnarsson, G., and Ingolfsdottir, A. (2005). Allegro version 2. Nat. Genet. *37*, 1015–1016.
10. Li, H., Ruan, J., and Durbin, R. (2008). Mapping short DNA sequencing reads and calling variants using mapping quality scores. Genome Res. *18*, 1851–1858.
11. Gilissen, C., Arts, H.H., Hoischen, A., Spruijt, L., Mans, D.A., Arts, P., van Lier, B., Steehouwer, M., van Reeuwijk, J., Kant, S.G., et al. (2010). Exome sequencing identifies *WDR35* variants involved in Sensenbrenner syndrome. Am. J. Hum. Genet. *87*, 418–423.
12. Tsurusaki, Y., Osaka, H., Hamanoue, H., Shimbo, H., Tsuji, M., Doi, H., Saitsu, H., Matsumoto, N., and Miyake, N. (2011). Rapid detection of a mutation causing X-linked leucoencephalopathy by exome sequencing. J. Med. Genet., in press. Published online March 17, 2011. 10.1136/jmg.2010.083535.
13. Becker, J., Semler, O., Gilissen, C., Li, Y., Bolz, H.J., Giunta, C., Bergmann, C., Rohrbach, M., Koerber, F., Zimmermann, K., et al. (2011). Exome sequencing identifies truncating mutations in human *SERPINF1* in autosomal-recessive osteogenesis imperfecta. Am. J. Hum. Genet. *88*, 362–371.
14. Fukuda, M. (2003). Molecular cloning, expression, and characterization of a novel class of synaptotagmin (Syt XIV) conserved from *Drosophila* to humans. J. Biochem. *133*, 641–649.
15. Adolfsen, B., Saraswati, S., Yoshihara, M., and Littleton, J.T. (2004). Synaptotagmins are trafficked to distinct subcellular domains including the postsynaptic compartment. J. Cell Biol. *166*, 249–260.
16. Quintero-Rivera, F., Chan, A., Donovan, D.J., Gusella, J.F., and Ligon, A.H. (2007). Disruption of a synaptotagmin (*SYT14*) associated with neurodevelopmental abnormalities. Am. J. Med. Genet. A. *143*, 558–563.
17. Michelsen, U., and von Hagen, J. (2009). Isolation of subcellular organelles and structures. Methods Enzymol. *463*, 305–328.
18. Fukuda, M., Kojima, T., and Mikoshiba, K. (1996). Phospholipid composition dependence of Ca^{2+}-dependent phospholipid binding to the C2A domain of synaptotagmin IV. J. Biol. Chem. *271*, 8430–8434.
19. Doi, H., Mitsui, K., Kurosawa, M., Machida, Y., Kuroiwa, Y., and Nukina, N. (2004). Identification of ubiquitin-interacting proteins in purified polyglutamine aggregates. FEBS Lett. *571*, 171–176.
20. Jana, N.R., Tanaka, M., Wang, G., and Nukina, N. (2000). Polyglutamine length-dependent interaction of Hsp40 and Hsp70 family chaperones with truncated N-terminal huntingtin: Their role in suppression of aggregation and cellular toxicity. Hum. Mol. Genet. *9*, 2009–2018.
21. Oyama, F., Miyazaki, H., Sakamoto, N., Becquet, C., Machida, Y., Kaneko, K., Uchikawa, C., Suzuki, T., Kurosawa, M., Ikeda, T., et al. (2006). Sodium channel beta4 subunit: down-regulation and possible involvement in neuritic degeneration in Huntington's disease transgenic mice. J. Neurochem. *98*, 518–529.
22. Gros-Louis, F., Dupré, N., Dion, P., Fox, M.A., Laurent, S., Verreault, S., Sanes, J.R., Bouchard, J.P., and Rouleau, G.A. (2007). Mutations in *SYNE1* lead to a newly discovered form of autosomal recessive cerebellar ataxia. Nat. Genet. *39*, 80–85.
23. McCue, H.V., Haynes, L.P., and Burgoyne, R.D. (2010). The diversity of calcium sensor proteins in the regulation of neuronal function. Cold Spring Harb. Perspect. Biol. *2*, a004085.
24. Bai, J., and Chapman, E.R. (2004). The C2 domains of synaptotagmin—partners in exocytosis. Trends Biochem. Sci. *29*, 143–151.
25. Chapman, E.R. (2008). How does synaptotagmin trigger neurotransmitter release? Annu. Rev. Biochem. *77*, 615–641.
26. Rickman, C., Craxton, M., Osborne, S., and Davletov, B. (2004). Comparative analysis of tandem C2 domains from the mammalian synaptotagmin family. Biochem. J. *378*, 681–686.
27. Bhalla, A., Chicka, M.C., and Chapman, E.R. (2008). Analysis of the synaptotagmin family during reconstituted membrane fusion. Uncovering a class of inhibitory isoforms. J. Biol. Chem. *283*, 21799–21807.
28. Zhang, G., Bai, H., Zhang, H., Dean, C., Wu, Q., Li, J., Guariglia, S., Meng, Q., and Cai, D. (2011). Neuropeptide exocytosis involving synaptotagmin-4 and oxytocin in hypothalamic programming of body weight and energy balance. Neuron *69*, 523–535.
29. Ellgaard, L., and Helenius, A. (2003). Quality control in the endoplasmic reticulum. Nat. Rev. Mol. Cell Biol. *4*, 181–191.
30. Colgan, S.M., Hashimi, A.A., and Austin, R.C. (2011). Endoplasmic reticulum stress and lipid dysregulation. Expert Rev. Mol. Med. *13*, e4.
31. Glavan, G., Schliebs, R., and Zivin, M. (2009). Synaptotagmins in neurodegeneration. Anat. Rec. (Hoboken) *292*, 1849–1862.
32. Schmitz-Hübsch, T., du Montcel, S.T., Baliko, L., Berciano, J., Boesch, S., Depondt, C., Giunti, P., Globas, C., Infante, J., Kang, J.S., et al. (2006). Scale for the assessment and rating of ataxia: Development of a new clinical scale. Neurology *66*, 1717–1720.

REPORT

De Novo and Inherited Mutations in *COL4A2*, Encoding the Type IV Collagen α2 Chain Cause Porencephaly

Yuriko Yoneda,[1] Kazuhiro Haginoya,[2,3] Hiroshi Arai,[4] Shigeo Yamaoka,[5] Yoshinori Tsurusaki,[1] Hiroshi Doi,[1] Noriko Miyake,[1] Kenji Yokochi,[6] Hitoshi Osaka,[7] Mitsuhiro Kato,[8] Naomichi Matsumoto,[1] and Hirotomo Saitsu[1,*]

Porencephaly is a neurological disorder characterized by fluid-filled cysts or cavities in the brain that often cause hemiplegia. It has been suggested that porencephalic cavities result from focal cerebral degeneration involving hemorrhages. De novo or inherited heterozygous mutations in *COL4A1*, which encodes the type IV α1 collagen chain that is essential for structural integrity for vascular basement membranes, have been reported in individuals with porencephaly. Most mutations occurred at conserved Gly residues in the Gly-Xaa-Yaa repeats of the triple-helical domain, leading to alterations of the α1α1α2 heterotrimers. Here we report on two individuals with porencephaly caused by a heterozygous missense mutation in *COL4A2*, which encodes the type IV α2 collagen chain. Mutations c.3455G>A and c.3110G>A, one in each of the individuals, cause Gly residues in the Gly-Xaa-Yaa repeat to be substituted as p.Gly1152Asp and p.Gly1037Glu, respectively, probably resulting in alterations of the α1α1α2 heterotrimers. The c.3455G>A mutation was found in the proband's mother, who showed very mild monoparesis of the left upper extremity, and the maternal elder uncle, who had congenital hemiplegia. The maternal grandfather harboring the mutation is asymptomatic. The c.3110G>A mutation occurred de novo. Our study confirmed that abnormalities of the α1α1α2 heterotrimers of type IV collagen cause porencephaly and stresses the importance of screening for *COL4A2* as well as for *COL4A1*.

Porencephaly (MIM 175780) is a neurological disorder characterized by fluid-filled cysts or cavities in the brain.[1] It has been suggested that porencephalic cysts are caused by a disturbance of vascular supply leading to cerebral degeneration.[2,3] Porencephaly clinically causes hemiplegia (most often), tetraplegia, epilepsy, and intellectual disability.[4,5] Monozygous twinning, maternal cardiac arrest or abdominal trauma, a deficient protein C anticoagulant pathway, or cytomegalovirus infections are risk factors for sporadic porencephaly.[2,6] Recently, mutations in the gene encoding type IV collagen α1 chain (*COL4A1* [MIM 120130]) have been shown to cause familial porencephaly.[7] Since then, de novo and inherited *COL4A1* mutations have been reported,[8–10] confirming that *COL4A1* abnormalities are involved in both sporadic and familial porencephaly. Type IV collagens are basement membrane proteins that are expressed in all tissues including the vasculature. COL4A1 (α1 chain) and COL4A2 (α2 chain) are the most abundant type IV collagens, and form heterotrimers with 2:1 stoichiometry (α1α1α2).[11] A mouse model of the heterozygous *COL4A1* mutation (*Col4a1*$^{+/\Delta ex40}$) showed cerebral hemorrhage and porencephaly and displayed abnormalities of vascular basement membranes, such as uneven edges, inconsistent density, and highly variable thickness.[7] In addition, a dominant negative effect of the *Col4a1*$^{+/\Delta ex40}$ mutation was demonstrated on collagen IV α1α1α2 heterotrimer assembly and its secretion.[7] In humans, most mutations are substitutions of the conserved Gly residue in the Gly-Xaa-Yaa repeat of the triple-helical domain, and they have a dominant negative effect on heterotrimer formation.[11,12]

COL4A2 (MIM 120090), which encodes the type IV α2 collagen chain, is a possible candidate for porencephaly because its mutations may affect the α1α1α2 heterotrimer. Supporting this idea, osteogenesis imperfecta type I-IV (MIM 166200, 166210, 259420, and 166220), which is characterized by abnormal bone fragility and low bone mass, is caused by mutations in both *COL1A1* (MIM 120150) and *COL1A2* (MIM 120160) that may interfere with formation of the collagen I α1α1α2 heterotrimer.[13] Moreover, mice lines harboring *Col4a2* point mutations (*Col4a2*^{ENU415}, c.227G>T [p.Val31Phe]; *Col4a2*^{ENU4003} and *Col4a2*^{ENU4020}, c.2073G>A [p.Gly646Asp]) showed abnormalities of the lens, cornea, and vascular stability.[14] In the brains of the mutants, pseudocysts in the upper cortical plate, hemorrhages surrounding small blood vessels, and focal hemorrhagic necroses were observed, indicating that *Col4a2* mutations cause abnormalities of the cerebral vasculature similar to those caused by *Col4a1* mutations.[7,14] In this study, we screened for *COL4A2* mutations in 35 Japanese individuals with porencephaly. Substitutions of a Gly residue in the Gly-Xaa-Yaa repeat were identified in two individuals (individuals 1 and 2). Clinical information and peripheral blood samples were

[1]Department of Human Genetics, Yokohama City University Graduate School of Medicine, Fukuura 3-9, Kanazawa-ku, Yokohama 236-0004, Japan; [2]Department of Pediatrics, Tohoku University School of Medicine, Seiryo-machi 1-1, Aoba-ku, Sendai 980-8574, Japan; [3]Department of Pediatric Neurology, Takuto Rehabilitation Center for Children, Akiu-machi 20, Taihaku-ku, Sendai 982-0241, Japan; [4]Department of Pediatric Neurology, Morinomiya Hospital, Morinomiya2-1-88, Joto-ku, Osaka 536-0025, Japan; [5]Department of Neonatal Medicine and Pediatrics, Osaka Medical College, 2-7 Daigakumachi, Takatsuki, Osaka 569-8686, Japan; [6]Department of Pediatric Neurology, Seirei-Mikatahara General Hospital, 2-12-12 Sumiyoshi, Naka-ku, Hamamatsu 430-8558, Japan; [7]Division of Neurology, Clinical Research Institute, Kanagawa Children's Medical Center, 2-138-4 Mutsukawa, Minami-ku, Yokohama 232-8555, Japan; [8]Department of Pediatrics, Yamagata University School of Medicine, Iida-nishi 2-2-2, Yamagata 990-9585, Japan
*Correspondence: hsaitsu@yokohama-cu.ac.jp
DOI 10.1016/j.ajhg.2011.11.016.

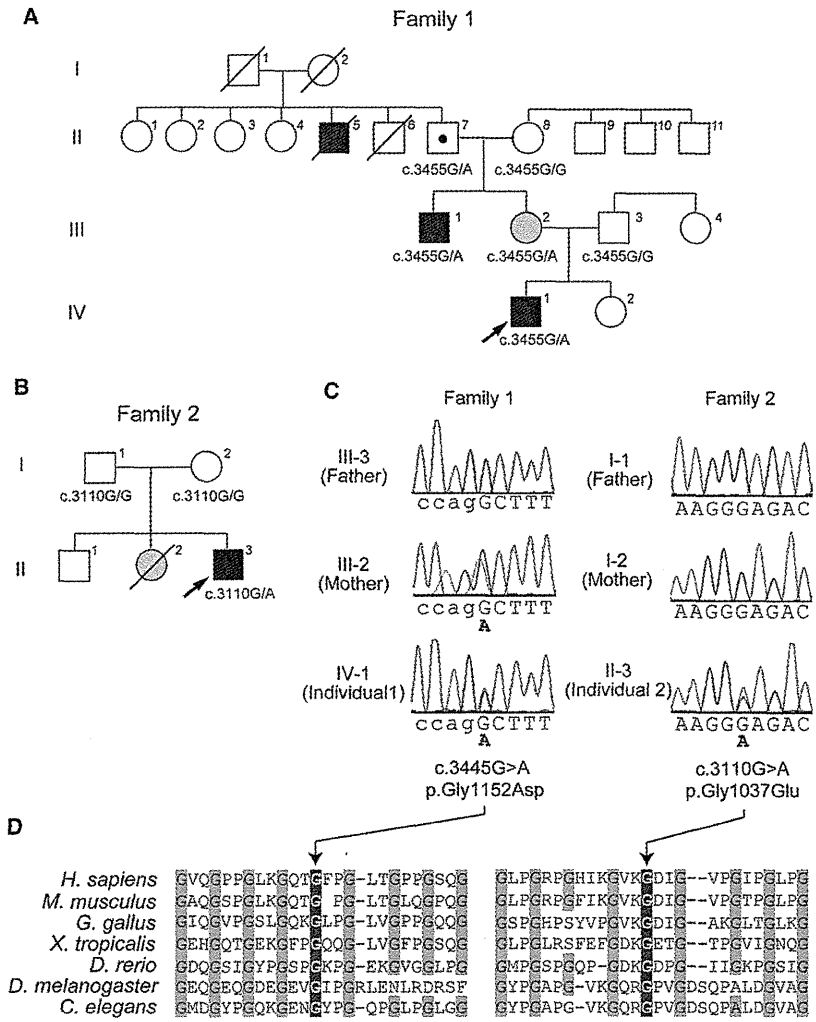

Figure 1. Pedigrees and *COL4A2* Mutations in Individuals 1 and 2

Pedigrees of family 1(A) and family 2 (B). The arrows indicate the probands (Individual 1 in family 1 and individual 2 in family 2). The segregation of the *COL4A2* mutations is shown. In family 1, the proband's mother (III-2) and maternal uncle (III-1) had mild monoparesis of the left upper extremity and congenital left hemiplegia and an assisted walk, respectively. The maternal grandfather (II-7) was healthy. The elder granduncle (II-5) was also afflicted by congenital hemiplegia and died in his 60s. (B) In family 2, the proband had a heterozygous mutation, but his parents did not have this mutation, indicating that the mutation occurred de novo. His elder sister (II-2) had intraventricular hemorrhage two days after birth but her DNA was unavailable.

(C) Electropherogram of family 1 (left) and family 2 (right). The intron and exon bases are in lower and upper cases, respectively. The c.3455G>A (p.Gly1152Asp) mutation in individual 1 was inherited from his mother. The c.3110G>A (p.Gly1037Glu) mutation in individual 2 occurred de novo.

(D) Multiple amino acid sequence alignments of COL4A2 proteins showing the evolutionarily conserved amino acids. The protein sequences obtained from the National Center for Biotechnology Information protein database are, NP_001837.2 (*Homo sapiens*), NP_034062.3 (*Mus musculus*), NP_001155862.1 (*Gallus gallus*), XP_002933063.1 (*Xenopus tropicalis*), XP_687811.5 (*Danio rerio*), AAB64082.1 (*Drosophila melanogaster*), and CAA80537.1 (*Caenorhabditis elegans*). The multiple sequence alignment was performed via the CLUSTALW website (see Web Resources). The positions of the conserved Gly residues in the Gly-X-Y repeats where the mutations occurred are highlighted with gray.

obtained from their family members after obtaining written informed consent. Experimental protocols were approved by the Institutional Review Board of Yokohama City University School of Medicine.

Individual 1 is 7 years old and a product of nonconsanguineous healthy parents (Figure 1A, arrow). There was no abdominal traumatism associated with the pregnancy and delivery in the mother. The individual was born at 36 weeks' gestation with a planned Caesarean section because, at 31 weeks' gestation, an antenatal ultrasound scan revealed an enlarged right lateral ventricle. Apgar scores were 9 at 1 min and 10 at 5 min. He weighed 2,900 g (+1.09 standard deviation [SD]) and had a head circumference of 32.5 cm (+0.05 SD). His early development was delayed with poor left hand use and abnormal leg movement. Brain magnetic resonance imaging (MRI) at 6 months showed an enlarged right lateral ventricle. Abrupt vomiting and nausea followed by motionless arrest developed at the 10 months. An electroencephalogram (EEG) showed focal spikes in the right frontal region, and carbamazepine treatment was initiated at the 12 months. Rehabilitation was started at 10 months. The individual started rolling at 12 months, crawling at 18 months, and walking alone at 3 years. He had spastic triplegia (diplegia and left hemiplegia) showing hemiplegic and diplegic gait with fluent speech and normal word comprehension. At the 5 years of age, he underwent orthopedic surgery for foot deformity due to spastic paresis. An EEG showed spikes in the right occipital to posterior temporal region and midcentral region. A brain MRI at age 6 showed an enlarged right lateral ventricle, reduced volume of the right frontal white matter, and atrophic right cerebral peduncle and body of corpus callosum (Figures 2A–2C). His intelligent quotient [IQ] score, evaluated at 6 years with Wechsler Intelligence Scale for Children-Third Edition (WISC-III), was 74 (his performance IQ was 69 and his verbal IQ was

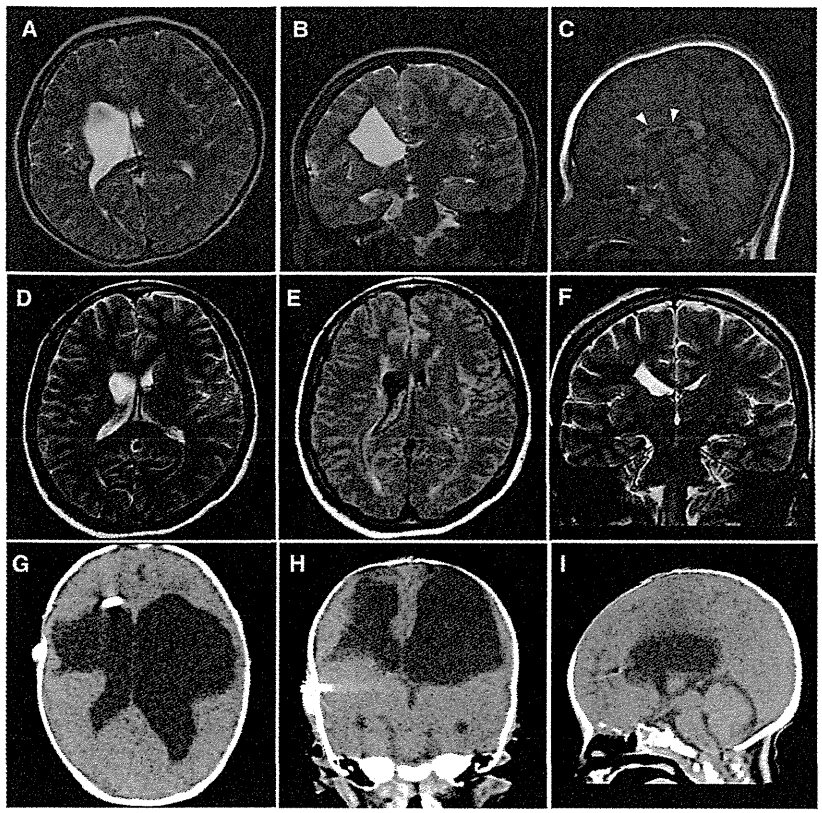

Figure 2. Brain Imaging in Individuals 1 and 2

(A–C) Brain MRIs of individual 1 at 6 years old; (A) T2-weighted axial image. (B) Coronal image. The images in (A) and (B) show an enlarged right lateral ventricle and a reduced volume of the right frontal white matter. (C) T1-weighted midline sagittal image showing atrophy of the body of the corpus callosum (arrowheads). The lesion responsible for the left leg paresis is not evident in these images.

(D–F) Brain MRIs of individual 1's mother at age 31. (D) T2-weighted axial and (F) coronal images show a mildly enlarged right lateral ventricle. (E) FLAIR axial image shows high signal intensity around the enlarged ventricular wall, which is consistent with mild porencephaly or periventricular venous infarction.

(G–I) CT images of individual 2 at 2 months of age. (G) Axial image. (H) Coronal image. (I) Sagittal image. The images in (G), (H), and (I) show an enlarged bilateral lateral ventricle and an extremely reduced volume of bilateral frontal white matter. The V-P shunt tube is also visible in the right lateral ventricle. The pontocerebellar structures seem to be normal.

82). The individual is now 7 years old and attending a local school. He can walk with ankle foot orthosis and hand assist. The epilepsy is well controlled with carbamazepine and clobazam. He does not show hematuria, muscular cramps, or ophthalmic abnormalities. His mother was born at term without asphyxia after an uneventful pregnancy. She had convulsions at the age of 18 months, and anticonvulsant was started under a diagnosis of focal epilepsy. Seizures were well controlled and treatment was discontinued at the age of 13. She first realized clumsiness of the left hand when she started learning piano and recorder at the age of 9. When she was a junior high school student, she felt severe headaches, and abnormal findings were pointed out in the brain MRI study (detailed information was unavailable). However, she did not undergo any more examinations because the headaches disappeared and did not recur. Neurological examination at 31 years revealed very mild monoparesis of the left upper extremity. She had neither spasticity nor exaggerated tendon reflexes. The grip power of her right and left hands was 25 and 15 kg, respectively. Mirror movement was observed on the right hand. The brain MRI revealed a mildly enlarged right lateral ventricle and high signal intensity around the enlarged ventricular wall on a Fluid Attenuated Inversion Recovery (FLAIR) image, which is consistent with mild porencephaly or periventricular venous infarction (Figures 2D–2F). MR angiography showed no aneurysms. Of note, his maternal elder uncle also showed congenital left hemiplegia with an assisted walk, and his maternal granduncle had also been afflicted by congenital hemiplegia, suggesting a genetic predisposition in the family (Figure 1A).

Individual 2 is 1 year and 4 months old and a product of nonconsanguineous healthy parents (Figure 1B, arrow). There was no abdominal traumatism associated with the pregnancy and delivery in the mother. He was born at 35 weeks' gestation. His birth weight was 1,694 g (−2.36 SD) and his head circumference was 29 cm (−1.77 SD). Mild asphyxia was observed, and he had Apgar scores of 3 at 1 min and 7 at 5 min. An ultrasound scan at 6 hr after birth revealed a parenchymal hemorrhage of the right cerebral hemisphere with an enlarged left lateral ventricle. Because a blood test revealed significant increases in prothrombin time (29.3 s) and activated partial thromboplastin time (104.3 s), but not in D-dimer (0.7 μg/ml) at 1 day after birth, he was treated with a daily infusion of fresh frozen plasma for 12 days. At 37 days after birth, he underwent a ventricular-peritoneal shunt (V-P shunt) operation for progressive enlargement of the lateral ventricle. Computed tomography (CT) at 2 months of age showed an enlarged bilateral lateral ventricle and an extremely reduced volume of bilateral frontal white matter (Figures 2G–2I). Blood coagulation was normalized at 7 months. At the 7 months, the individual did not show any head control or rolling, and presented with abnormal posturing and spastic quadriplegia dominant on the left side of his body. With